Title:

Modeling the Global Emission, Transport and Deposition of Trace Elements Associated with Mineral Dust

Authors:

Y. Zhang [yan_zhang@fudan.edu.cn]
N. Mahowald [mahowald@cornell.edu]

R. A. Scanza [ras486@cornell.edu]

E. Journet [emilie.journet@lisa.u-pec.fr]

K. Desboeufs [karine.desboeufs@lisa.u-pec.fr]

S. Albani [s.albani@cornell.edu]

J. F. Kok [jfkok@ucla.edu]

G. Zhuang [gzhuang@fudan.edu.cn]

Y. Chen [yingchen@fudan.edu.cn]

D. D. Cohen [dcz@ansto.gov.au]

A. Paytan [apaytan@ucsc.edu]

M. D. Patey[mpatey@gmail.com]

E. P. Achterberg [eachterberg@geomar.de]

J. P. Engelbrecht [Johann.Engelbrecht@dri.edu]

K. W. Fomba [fomba@tropos.de]

Modeling the Global Emission, Transport and Deposition of Trace Elements Associated with Mineral Dust

Yan Zhang[1,2], Natalie Mahowald[2], Rachel Scanza[2], Emilie Journet[3], Karine Desboeufs[3], Samuel Albani[2], Jasper F. Kok[4], Guoshun Zhuang[1], Ying Chen[1], David D. Cohen[5], Adina Paytan[6], Matt D. Patey[7], Eric P. Achterberg[7,9], Johann P. Engelbrecht[8], KhannehWadinga Fomba[10]

1. Shanghai Key Laboratory of Atmospheric Particle Pollution and Prevention (LAP[3]), Department of Environmental Science and Engineering, Fudan University, Shanghai, China
2. Department of Earth and Atmospheric Science, Cornell University, Ithaca, NY, USA
3. LISA, UMR CNRS 7583, Université Paris-Est Créteil et Université Paris-Diderot, Créteil, France
4. Department of Atmospheric and Oceanic Sciences, University of California, Los Angeles, CA, USA
5. Australian Nuclear Science and Technology Organization, Locked Bag 2001, Kirrawee DC, NSW, 2232, Australia
6. Earth and Planetary Sciences Department, University of California, Santa Cruz, CA 95064, USA.
7. Ocean and Earth Science, National Oceanography Centre Southampton, University of Southampton, Southampton SO14 3ZH, UK
8. Desert Research Institute (DRI), 2215 Raggio Parkway, Reno, Nevada 89512-1095, USA
9. GEOMAR, Helmholtz Centre for Ocean Research, 24148 Kiel, Germany
10. Leibniz Institute for Tropospheric Research (TROPOS), 04318 Leipzig, Germany.

Abstract Trace element deposition from desert dust has important impacts on ocean primary productivity, the quantification of which could be useful in determining the magnitude and sign of the biogeochemical feedback on radiatiave forcing. However, the impact of elemental deposition to remote ocean regions is not well understood and is not currently included in global climate models. In this study, emission inventories for eight elements primarily of soil origin, Mg, P, Ca, Mn, Fe, K, Al, and Si are determined based on a global mineral dataset and a soil dataset. The resulting elemental fractions are used to drive the desert dust model in the Community Earth System Model (CESM) in order to simulate the elemental concentrations of atmospheric dust. Spatial variability of mineral dust elemental fractions is evident on a global scale, particularly for Ca. Simulations of global variations in the Ca/Al ratio, which typically range from around 0.1 to 5.0 in soils, are consistent with observations, suggesting that this ratio is a good signature for dust source regions. The simulated variable fractions of chemical elements are sufficiently different; estimates of deposition should include elemental variations, especially for Ca, Al and Fe. The model results have been evaluated with observations of elemental aerosol concentrations from desert regions and dust events in non-dust regions, providing insights into uncertainties in the modeling approach. The ratios between modeled and

observed elemental fractions range from 0.7 to 1.6, except for Mg and Mn (3.4 and 3.5, respectively). Using the soil database improves the correspondence of the spatial hetereogeneity in the modeling of several elements (Ca, Al and Fe) compared to observations. Total and soluble dust element fluxes to different ocean basins and ice sheet regions have been estimated, based on the model results. Annual inputs of soluble Mg, P, Ca, Mn, Fe and K associated with dust using the mineral dataset are 0.28 Tg, 16.89 Gg, 1.32 Tg, 22.84 Gg, 0.068Tg, and 0.15 Tg to global oceans and ice sheets.

Key word: dust; Ca/Al ratio; dust; minerals; atmospheric deposition; global model

1 Introduction

Desert dust aerosols are soil particles suspended in the atmosphere by strong winds, and originate primarily from regions with dry, un-vegetated soils. Desert dust particles are thought to contain several important chemical elements, which can impact the earth system by influencing biogeochemical cycles, in particular, marine primary productivity (Martin et al., 1991; Duce and Tindale. 1991;Herut et al., 1999, 2002, 2005; Okin et al., 2004; Jickells et al., 2005). Iron (Fe) is considered the most important element carried in dust, and low Fe supplies combined with a low dust solubility are thought to limit phytoplankton growth in High Nutrient Low Chlorophyll (HNLC) regions. The HNLC regions feature residual macronutrient (e.g. nitrogen (N) and phosphorus (P)) concentrations, but productivity remains limited by the low supply of Fe (e.g. Martin et al.,1991; Boyd et al., 1998). Further studies have linked Fe to the nitrogen cycle because of high Fe requirements of N fixing organisms (e.g. Capone et al., 1997). While there are internal sedimentary sources of Fe in the ocean, dust deposition is an important source of new Fe to remote regions of the ocean (e.g. Fung et al., 2000, Lam and Bishop, 2008; Moore and Braucher, 2008). Desert dust also contains P, which is a limiting nutrient in some ocean and land regions (e.g. (Mills et al., 2004; Okin et al., 2004; Swap et al., 1992)), especially on longer time scales. In addition, as a dominant constituent of mineral dust, silicon (Si) is an important nutrient for diatoms which are central in ocean productivity (Morel et al., 2003). Other elements released from mineral dust which may be important for ocean biogeochemistry including manganese (Mn) as a biologically essential nutrient and aluminum (Al) as a tracer of atmospheric inputs (e.g. Nozaki, 1997; http://www.geotraces.org/science/science-plan).

Previous studies have emphasized the importance of measuring elemental composition of dust elements (Kreutz and Sholkovitz, 2000; Cohen et al., 2004; Marino et al., 2004; Marteel et al., 2009), and there are a range of studies highlighting observations of elemental distributions and ecosystem impacts (e.g. Baker et al., 2003;Herut et al., 2002; Buck et al., 2006; Paytan et al., 2009; Chen and Siefert, 2004; Measures and Vink, 2000). In-situ observations show evidence of heterogeneities in elemental fractions over arid soil regions (Svensson et al.,2000;Zhang et al., 2003; Shen et al., 2005, 2006; Li et al., 2007). Ratios between elements including Si, Al, Mg, Ca, and in particular Ca/Al ratios have also been used to distinguish dust source regions,

for example the Asian desert (Zhang et al., 1996; Sun et al., 2005; Han et al., 2005; Shen et al., 2007) and African deserts (Bergametti et al., 1989;Formenti et al., 2008).

Xuan (2005) has simulated the emission inventory of trace elements in the dust source regions of East Asia. However, there has not yet been a study to model the distribution of dust-associated elements on a global scale. Global dust models usually assume a fixed fraction (e.g. normalized to Al) of each element in dust to simulate global dust elemental transport and deposition. For example, Fe is thought to contribute 3.5% and P 0.075% to mineral dust (by mass) (e.g. Luo et al., 2008; Mahowald et al., 2008). Besides spatial variations in elemental compositions, particle size distribution forms another important determinant of elemental abundance in deposited dust. Depending on the particle size distribution, trace elements may remain more or less suspended in the atmosphere and deposited by dry or wet deposition at various distances from desert regions (Seinfeld and Pandis, 1998). There have been very few studies investigating particle size distribution and elemental concentrations in soil and dust by direct measurement (Schütz and Rahn, 1982; Reid et al., 2003; Castillo et al., 2008; Engelbrecht et al., 2009a,b), and even fewer modeling studies have included this. The ability to model the deposition of specific elements associated with dust in global simulations has been hindered by a lack of understanding of the spatial and temporal variability, as well as the particle size distribution associated with different dust sources. As noted by Lawrence and Neff (2009), it seems most appropriate to use a globally averaged value of dust composition to estimate the elemental flux from dust, given the lack of direct measurements of the spatial distribution of elements in dust. However, the use of a global mineral map (Claquin et al., 1999; Nickovic et al. 2012, 2013; Journet et al., 2014) and chemical compositions of minerals (Journet et al., 2008) allows us to simulate global elemental inventories from mineral soils, which could be used in a global dust model.

This study aims to introduce a technique to determine a size-fractionated global soil elemental emission inventory based on two different datasets, a global soil dataset and a mineralogical dataset. A companion paper evaluates the ability of the model to simulate mineralogy and the impact on radiation (Scanza et al., 2015). The elemental emission dataset estimated for Mg, P, Ca, Fe, Mn, K Al, and Si was used as an input to a model simulation of the global dust cycle to present the elemental distributions, which were compared against available observations of concentration and deposition to different ocean regions.. Our goal is to assess the variability of elemental fractions in atmospheric and deposited dust, and to investigate whether the elemental emission dataset can adequately predict this variability. This study focuses on desert dust particles, and thus disregards other potentially important sources of the elements such as combustion processes (e.g. Guieu et al., 2005; Luo et al., 2008; Mahowald et al., 2008). We focus on total elemental concentrations, but discuss two methodologies for soluble metal distributions from soil emissions. We also do not consider any atmospheric processing, which is likely to be important for some chemical components (e.g. Mahowald et al., 2005; Baker and Croot, 2010).

2 Materials and Methods

2.1 Soil and mineral datasets

The soil map of the world used in this study comes from the Food and Agriculture Organization (FAO) of the United Nations soils dataset, and includes 136 soil units [FAO-United Nations Educational, Scientific, and Cultural Organization (FAO-UNESCO, 1995) at a 5-minute resolution. The global dataset of soil clay and silt data are used in this study. Following Claquin et al. (1999) and Nickovic et al. (2012), the illite, hematite, kaolinite, smectite, quartz, feldspars, calcite and gypsum contents are specified for different clay and silt soil types, and the global mineral distribution is presented in Scanza et al (2015). Some minerals found in dust such as dolomite were not considered by Claquin et al. (1999) and Nickovic et al. (2012) and have also been disregarded in this study due to the lack of data on their distribution.

The elemental compositions of hematite and aluminosilicate minerals used in this study are taken from previous works (Journet et al. (2008) and unpublished data provided by E. Journet, 2012) and were obtained by X-ray fluorescence spectrometry (XRF) (Table 1a). Most of minerals used by Journet et al. (2008) are reference materials from the Society's Source Clays Repository, i.e. hematite, illite, kaolinite, montmorillonite. The elemental compositions obtained by XRF are in the range of published values for these reference materials (e.g. Mermut and Cano, 2001; Gold et al., 1983), validating the obtained composition for the unreferenced materials. Moreover, the purity of all minerals samples is estimated by X-Ray diffraction. Note that the mineralogical maps used in this study do not distinguish feldspar and smectite subtypes. For feldpars, the elemental composition is mostly averaged based on 2 subtype minerals: orthoclase (potassic feldspar) and oligoclase (sodium-calcium feldspar). For smectites, the montmorillonite subtype is the most commonly identified smectite in desert dust, particularly for Saharan dust e.g. Goudie and Middleton, 2006). The chemical composition of montmorillonite is used in this study as an analog for smectite. For calcite, gypsum, and quartz, the natural minerals could contain substitutions or impurities from clays, which are variable depending on origin, formation, contamination, etc. of minerals. Because regional silt samples were not available for spectroscopy, we use the theoretical composition of elements in calcite, gypsum and quartz (Table 1a). The mass fraction of Ca in calcite ($CaCO_3$) and gypsum ($CaSO_4 \bullet 2H_2O$) are taken as 40% and 23.3%, respectively. A mass fraction of 46.7% Si is used for pure quartz (SiO_2).

Following the total element calculation, soluble elemental fractions are estimated based on soluble elemental contents of minerals at pH=2 reported by Journet et al (2008) for hematite and the aluminosilicates, and is listed in Table 1b. The fractional solubility of Ca in calcite and gypsum used is 7% and 0.56%, respectively, and that of Si in quartz was 0.0003% based on individual solubility product (K_{sp}) at pH=2 (Petrucci et al., 2001). Here the mineral dependent method used to calculate soluble elements is defined as Method 1 (Sol-1). To present uncertainties, another approach (Method 2, defined as Sol-2) is introduced as a reference. It is based on the extractable elemental fractions of in-situ 20 μm sieved soil samples reported by Sillanpaa (1982) (Table S1) and is combined with an FAO soil dataset to get a global soluble elemental inventory independent of soil minerals. It is noted that there is no detailed size distribution for soil samples in Sol-2. Thus, the fractions of soluble elements in clay and silt are assumed to be equal to that of the bulk soils themselves.

Table S1Averaged macronutrient contents (‰) of soils classified by FAO/Unesco soil units *

One drawback of our approach is that we disregard the large variability of soils included within each defined "soil type". The range of minerals within each soil type is large (e.g. Claquin et al., 1999), and the range of elemental concentrations in each mineral is also large (Journet et al., 2008). The resolution of our model is such that despite the actual heterogeneity of soils at a particular location, we prescribe an average at each gridbox which tends to reduce the variability in elemental composition in the mineral dust in the atmosphere. This is likely to be the largest source of uncertainty in our approach.

Table1 (a) Generalized mineral compositions (%) applied in this study ;(b) Elemental solubility as a percentage of the element contained in the minerals (%)

Table 2 Emission rates (Tg/yr) and percentages of elements over desert regions (%)

2.2 Numerical Model description

Community Earth System Model version 1.0.3 (CESM1.0.3) is coordinated by the National Center for Atmospheric Research (NCAR), and has been used to simulate elemental dust emission, transport and deposition in this study. The bulk mineral aerosol in the Community Atmosphere Model version 4 (CAM4) was adapted to include eight trace elements within total dust (Scanza et al., 2015). In this model simulation, the physical scheme CAM4 is driven by the meteorological dataset MERRA, and is simulated spatially at 1.9×2.5 degree resolution for the years 2000-2010. The soil erodibility map used by the dust model has been spatially tuned (Albani et al.,2014). There are four size classes of dust particles used in the dust emission module in the bulk scheme with particle diameters of 0.1-1.0, 1.0-2.5, 2.5-5.0 and 5.0-10.0 μm. The sub-bin size distribution is assumed to follow a log-normal distribution with a mass median diameter of 3.5 μm (Mahowald et al., 2006) and a geometric standard deviation of 2.0 μm (Zender et al., 2003). Combining these log-normal parameters with the brittle fragmentation theory of dust emission (Kok, 2011) yields each bin's partitioning of dust aerosol mass between the soil's clay and silt size fractions (see Table B3 and Scanza et al., 2015). The elements in the dust undergo three-dimensional transport individually in each of the different size bins, identically to bulk dust in the original model. Elemental atmospheric mixing ratios, and wet and dry deposition are updated at each model time step based on actual elemental fields and the corresponding tendencies.

By splitting the dust into its different mineral elements, we may add additional numerical errors, because the elements are transported separately. There has been considerable work on improving advection algorithms in atmospheric models, and here we use the finite volume advection algorithm as part of the CAM [*Lin and Rood*, 1997]. While no advection scheme is perfectly mass conserving, monotonic, shape preserving and computationally efficient, this scheme does a good job of balancing these multiple goals and maintaining the strong gradients required in modeling atmospheric constituents (e.g. [*Rasch et al.*, 2006]). Studies focused on elemental distributions in ocean models have suggested the relatively small uncertainties associated with these types of numerical errors (e.g. [*Christian*, 2007]), and compared with the errors in the source distribution of the minerals, errors from advection are likely to be small and are neglected here.

Table S2. The fraction of dust aerosol mass contributed by the soil clay and silt fractions for each of the 4 particle size bins for the bulk scheme in CAM4.

2.3 Observational data

An element dataset of ground based aerosol measurements at 17 sites (Table B3) is used to evaluate the elemental dust simulation (Sun et al., 2004a,b;Wang et al., 2010;Chen et al., 2008; Engelbrecht et al., 2009; Carpenter et al., 2010; Cohen et al., 2011;Guo et al., 2014; Formenti et al., 2008; Desboeufs et al., 2010). The sites are close to major dust-producing regions (Figure 1), including 10 Asian sites (Central Asia: Hetian, Tazhong; East Asia: Yulin, Duolun, Shengshi;South Asia: Hanoi, and Marnila; Middle East: Balad, Baghdad, Taji), 5 African sites (West Africa: Cape Verde Atmospheric Observatory (CVAO); East Africa: Eilat; North Africa: Tamanrasset, Banizoumbou, and Douz), and 2 Australian sites (Muswellbrook, Richmond). Generally, these field aerosol samples (Total Suspended Particulates (TSP), PM_{10}, $PM_{2.5}$) have 1-3 day collection periods during the period 2001-2010, and were chemically analyzed for elemental composition. No observational aerosol mass concentrations at the Cape Verde station could be used in this study. At this site, the particulate matter (PM) concentrations are estimated by assuming an Al to total dust mass ratio of 0.0804. In order to be certain that only desert dust elements are compared with the model results, only data collected during dust storm seasons are selected. Measurement sites from which data are taken are listed in Table B3, which includes related methodological details.

In addition, the dataset of dust deposition at more than 100 sites worldwide is used to evaluate modeled dust deposition fluxes (Albani et al., 2014).

Fig.1. Observational sites (S1-Hetian, China; S2-Tazhong, China; S3-Yu Lin, China; S4-Duolun, China; S5-Shengsi, China; S6-Hanoi, Vietnam; S7-Marnila, Philippines; S8- Balad, Iraq; S9-Balad, Iraq; S10-Taji, Iraq; S11-Eilat; S12-Cape Verde Atmospheric Observatory (CVAO); S13-Muswellbrook, Australia; S14-Richmond, Australia; S15-Tamanrasset, Algeria; S16-Banizoumbou, Niger; S17-Douz, Tunisia) **and dust-producing regions** (WAsia: West Asia; NC-As: North Central Asia; CAsia: Central Asia; SC-As: South Central Asia; EAsia:East Asia; WN-Af:North West Africa; EN-Af: North East Africa; S-NAf: Southern North Africa; SAf: Southern Africa; MNWAm: Middle North West America; SNWAm: Southern North West America; SAm1: Northern South America; SAm2: Southern South America; WAus: West Australia; EAus: East Australia)

Table S3. Locations of 17 sampling sites

3 Results and Discussion

3.1 Fractions of element in arid soil regions

The global distributions of the elements Mg, P, Ca, Mn, Fe, K, Al, and Si in bulk soils as mass percentages in soils are presented in Fig. 2.

3.1.1 Global mapping of soil associated elements

Fractions of elements in soils vary between mineralogical clay and silt fractions. Spatial variability of soil chemistry is seen on a global scale (Fig.2). A large range of variability for some elements within one given source region is observed (e.g. Ca, Fe, Mn, Al). The most extreme variability is observed for Ca in soil silt, which varied from 0.5 to 34.3%, and is much higher in West and Central Asia, South Africa and Northern South America than in other parts in the world. This is ascribed to the presence of feldspar and gypsum, both being important source minerals for Ca in these regions. In Central and East Asia, the Ca content increased from east to west, showing a similar spatial trend to that reported by Xuan et al. (2005). A south to north gradient of Ca content was also observed in the Sahara following the carbonate distribution of soils (Kandler et al., 2007; Formenti et al., 2011). In southern North Africa, South Africa and the Western Australia, clay soil and fine dust emissions have higher Al and P concentrations than elsewhere. In Eastern Australia, Patagonia, and the northern South Africa, the Fe content of soils is also higher than in other regions. Due to their high content of quartz, soils generally have 25-40% Si. These elemental distributions are in agreement with other published data for Fe, as they are derived from similar regions (e.g. Claquin, 1999; Hand, 2004).

Fig.2 Global elemental distributions (in mass percentage) in a1: Clay Mg, a2: Clay P, a3: Clay Ca, a4: Clay Mn, a5: Clay Fe, a6: Clay K, a7:, Clay Al, a8: Clay Si; b1: Silt Mg, b2: Silt P, b3: Silt Ca, b4: Silt Mn, b5: Silt Fe, b6: Silt K, b7: Silt Al, b8: Silt Si.

3.1.2 Elemental composition of soils and airborne dust

Trace elements in soils show different associations with particle size patterns depending on the size distribution of soil minerals. For example, Mg, P, Fe, Mn, and Al are dominant in the clay size fraction (< 2 μm) (Fig. 3b). Fractions of Al and Fe reach 11.7% and 3.1% in clay fractions of soils, while only 2.8% and 1.2% in silt fractions of soils, respectively. However, Ca and Si show a slight enrichment in coarser soil fractions. Ca comprises 2.6% of soils in the clay fraction but 3.6% in the soil silt fractions. This is consistent with the size distribution of Ca and Fe-rich individual particle groupings measured in Saharan dust (Reid et al., 2003). K has nearly equal distributions in clay and silt fractions of soils. Taking the fractions of elements in soils as inputs, the fractions of elements in dust emission can be predicted. Our classification of soil particles into four aerosol sizes (Table B2) provides heterogeneity in elements across sizes, but allows for a mixing across soil sizes, reducing the differences among size fractions. For example, the percentage of Fe remains unchanged from clay soil to fine mode dust emission, but changes substantially from silt soil (1.2%) to coarse mode dust (2.2% in Bin 3). A similar pattern appeares for the other elements, and the differences between elemental percentages in the soils are reduced when dust emissions are considered (Fig. 3a vs. 3b).

Fig.3 Global mean elemental percentages in (a) four-bin dust emission and (b) clay and silt fractions of soils (Bin1-4 refer to particle range listed in Table S2, clay refer to < 2um, silt refer to > 2um)

3.1.3Elemental dust emissions over desert regions

Annual elemental dust emissions over 15 dust-producing regions (shown in Fig.1) are determined (Table 2). The annual average of total global dust emission is estimated to be 1582 Tg based on 2001-2010 simulations,

and is within the wide range (514 to 5999 Tg/yr) as reported by previous studies (e.g. Textor et al., 2006, 2007;Prospero et al., 2010; Huneeus et al., 2011). Africa and Asia account for 68% and 31% of the global emissions, respectively. Correspondingly, trace element emissions are dominant from African desert regions, with percentages ranging between 65%-70%. Specifically, Al emission from Africa account for 70% of global Al emissions, of which 64% originated from the Western Sahara. For Asian desert regions, elemental dust account for 29-34% of the global total amount, with Ca being the strongest contributor (34%) to global Ca emissions. The percentage of Fe is similar to Al in the total dust emissions with 67% and 32% of Fe from Africa and Asia, respectively. The maximum % element for Ca at 5% was in dust emission from West Asia, being more than 4 times higher than Southern North Africa (1.2%). However, the fraction of Al and Si is largest in dust emission from Southern North Africa, with values of 9.0% and 31%, respectively. The fractions of Fe and P are 2.8%, and 0.08% in Australia, which is higher than that in other source regions. The simulated elemental fractions in dust suggest that differentiating elements in soils between global source areas is necessary and meaningful.

Table 2 Emission rates (Tg/yr) and elemental composition of dust over desert regions (%)

3.2 Spatial and seasonal distribution in fractions of elements in atmospheric and deposited dust

3.2.1 Elemental fractions in global atmospheric dust and deposited dust

The modeled fractions of different elements in atmospheric dust have substantial spacial variability (Fig. 4). Fe content is greater than 2% for most regions, with a global mean of 2.7% in atmospheric dust. The maximum contributions of Fe, Al, P and Mn fractions are observed in the tropical Pacific region with values greater than 3%, 10%, 0.08%, and 0.02%, respectively. For Ca, Si and K, a higher fraction is evident in terrestrial environments. There are obvious land-ocean gradients existing in the distributions of elemental fractions, with higher Ca and Si fractions in terrestrial regions and higher P, Fe, and Al fractions in oceanic areas, likely due to their differences in particle size distribution (Fig. 3). There are very similar spatial patterns and magnitudes shown for the elemental fractions in deposited dust compared with those in atmospheric dust for each element (Fig. S1, Fig. 5). Higher fractions of Ca and Si in deposited dust is observed in regions close to desert dust sources where the two elements occur in the coarser size fractions. Conversely, lower Mg, P, Mn, Fe and Al contents are found in dust deposits close to source regions but higher contents are found over oceans, which is consistent with the clay soil fraction dominating the finer particle size fractions. The importance of relative location of the source compared to the deposition to the elemental ratio adds complexity in applying simple percentages to dust deposition to obtain elemental deposition amounts.

Fig.4 Percentages of elements in dust concentration （mass %）: a. Mg, b. P, c. Ca, d. Mn, e. Fe, f. K, g. Al, h. Si. Elemental % shown here are calculated using the annual mean element concentration divided by the annual mean dust concentration.

Fig.S1 Percentages of elements in deposited dust（%）:a. Mg, b. P, c. Ca, d. Mn, e. Fe, f. K, g. Al, h. Si. Elemental annual mean % are calculated using the annual mean emission of each element divided by the annual mean emission of dust.

Fig.5 Ratio of mass fractions of elements in dust deposition to that in atmospheric dust : a. Mg, b. P, c. Ca, d. Mn, e. Fe, f. K, g. Al, h. Si. Elemental ratios shown here are calculated using the annual mean element deposition divided by the annual mean dust deposition.

3.2.2 Seasonal variability of elemental fractions

As described above, the fractions of elements in dust fluctuate temporally and spatially on a global scale. There are seasonal variations in dust emissions from various desert regions showing different emission patterns (Fig.S2). The peak periods for dust emissions for various desert regions are consistent with those found by Werner et al., (2002) (Figure S2). Combining the seasonal cycles in atmospheric dust production with the element distributions in desert regions, the elemental fractions show large monthly variability but small inter-annual variability during 2001-2010 (Fig. A3). Ca and Al have clear seasonal cycles, with Ca having the largest monthly variability with peak concentrations in the between July and September. This is ascribed to the higher Ca content of dust originating in West Asia, Central Asia and Southern Africa, regions that provide large global dust emissions in this period (JJAS).. For the other elements, the peak concentrations usually occurred between March and May (MAM) or November through January (NDJ), corresponding to the periods when global dust emissions reach a maximum.

We modeled the seasonal variability of these elemental fractions. Elemental percentages are calculated using the climatological monthly mean emission of each element divided by the climatological monthly mean emission of dust. An index describing monthly variability is calculated by:

$$Monthly\ variability\ (\%) = \frac{SD\ of\ mean\ fraction_{month}}{Mean\ \ fraction_{month}} \times 100 \qquad \text{(Eq. 1)}$$

Twelve monthly mean fractions are averaged from the ten year simulation, with the corresponding standard deviations (SDs).. Finally, the percentages (Eq.1) of the standard deviation in the monthly means is derived to describe the variability in elemental fractions of atmospheric dust and deposited dust (Fig. 6 and 7).

The monthly mean variation is greatest for Ca, reaching more than 30% variability in some regions. The temporal variability of elemental percentages in deposited dust tended to be larger than those in atmospheric dust and show a greater spatial gradient from land to sea. That is similar to the trend of the elemental fractions in atmospheric and deposited dust (section 3.2.1) since the temporal variation is originally induced by the

spatially variable elemental fraction. In the South Indian Ocean and the South Atlantic Ocean, the monthly variability is even higher and is attributed to the combined effect of variability in dust emissions, spatial .,elemental concentration, and dust transport patterns.

Fig.S2 Monthly dust emission (kg/m^2/s)over 15 dust-producing regions (WAsia: West Asia; NC-As:North Central Asia; CAsia:Central Asia; SC-As: South Central Asia; EAsia:East Asia; WN-Af:North West Africa; EN-Af: North East Africa; S-NAf: Southern North Africa; SAf: Southern Africa; MWNAm: Middle North West America; SWNAm: Southern North West America; SAm1: Northern South America; SAm2: Southern South America; WAus: West Australia; EAus: East Australia)

Fig.S3 Seasonal cycle of global mean elemental percentages (%) in atmospheric dust from 2001 to 2010. Elemental % are calculated using the climatological monthly mean emission of each element divided by the climatological monthly mean emission of dust.

Fig.6 Ten-year monthly variability in mean of elemental percentages in atmospheric dust (mass %) : a. Mg, b. P, c. Ca, d. Mn, e. Fe, f. K, g. Al, h. Si. Elemental monthly mean % are calculated using the monthly mean emission of each element divided by the monthly mean emission of dust.

Fig.7 Ten-year monthly variability in mean of elemental percentages in dust deposition (mass %):a. Mg, b. P, c. Ca, d. Mn, e. Fe, f. K, g. Al, h. Si. Elemental monthly mean % are calculated using the monthly mean emission of each element divided by the monthly mean emission of dust.

3.3 Spatial Ca/Al distribution in soils and dust plumes

Of specific interest is the Ca/Al ratio in soil, atmospheric dust and deposited dust as this ratio may be indicative of specific source regions (Fig. 8). Of all considered ratios, the Ca/Al ratio in soils show the greatest variability in relation to the relevant desert region (e.g. Formenti et al. (2011)). The Ca/Al ratio ranges mainly between 0.1-1 in clay fractions of soils and 0.5-5.0 in silt fractions of soils (Fig. 8a,b). The maximum Ca/Al ratios reaches 160 times the global mean Ca/Al ratio of 1.96 in the silt fraction of soils (Fig. 8b), much higher than those of other ratios such as Fe, K, and Mn to Al. Asian desert soils have higher Ca/Al ratios, with values greater than 5 in West Asia and Central Asia. The Ca/Al ratio in dust emissions from Central Asia (1.0-1.6) are higher than in East Asia (~0.5), which is close to Ca/Al ratios (1.0-1.7) derived from source profiles of Asian dust (Zhang et al., 1997; Zhang et al., 2003), and also match the observed Ca/Al ratios (0.7-1.3) during Asian dust events (Sun et al., 2004a,b; Shen et al., 2007). In addition, the Ca/Al ratio in dust emissions in North Africa are below 0.5, confirming the application of the Ca/Al ratio of 0.3 (or 3.8 with Al/Ca) as an indicator of North African dust transport to the eastern United States (Perry et al., 1997). Ambient $PM_{2.5}$ dust measured on the Canary Islands suggests a different ratio (Ca/Al = 1.004) (Engelbrecht et al., 2014). However, this ratio could be larger for PM_{10} or TSP. The high Ca/Al ratio (4.0-10.0) in a range of desert soils in some regions including South Africa, yields a Ca/Al ratios in dust emissions of 1.0, being much larger than those from North Africa. The modeled spatial pattern of Ca/Al ratio in dust emissions from Asia and northwest Africa is consistent with the currently available dust pattern compiled by Formenti et al. (2011), but shows relatively lower values for the Central Asian desert region.

Despite experiencing mixing of airborne dust from various source regions and as a result of dust processing during transport, the Ca/Al ratios still show spatial variations in global atmospheric dust and deposited dust. Relative to the Ca/Al ratio in source regions (Fig. 8a,b), the Ca/Al ratio in atmospheric dust over most of

terrestrial Asia ranges between 0.5-0.8, with a maximum of 1.8. This is due to the spatial variability of Ca/Al ratio in dust emissions (Fig. 9a) and despite the preferential gravitational settling during transport of silt fraction which represents the highest Ca/Al variability. The variability in Ca/Al ratio in dust deposited into oceans and onto ice sheets are also shown in Fig. 9b. Near West Asia and Western Sahara, higher Ca/Al ratios are noted and the North Indian ocean and Mediterranean sea have a Ca/Al ratio above 0.65 in deposited dust. As the combined downwind region of central Asia and East Asia, the North Pacific has a Ca/Al ratio around 0.5. The Ca/Al ratio in dust deposited over the Atlantic ranges between 0.3-0.4 due to the influence of southern North Africa desert region and East Sahara desert both with low ratios of Ca/Al. Since the soil dataset has a high spatial resolution of 5 arc minutes (Fig. 8a,b), there is opportunity to increase the model grid resolution ($1.9 \times 2.5°$ in this study) to a finer resolution. It is expected that Ca/Al ratio will show more spatial heterogeneity when a finer model resolution is used. We conclude that the Ca/Al ratio can be used to identify different source areas and the model can be used to support the observations.

Fig.8 Ca/Al in Soil and ten year averaged Ca/Al ratio in dust emission, concentration and deposition. Top two (a,b) refer to ratio in clay and silt desert soil, middle one (c) refer to ratio in dust emission, and bottom two (d,e) refer to ratio in dust concentration and deposition. Elemental annual mean % are calculated using the annual mean emission of each element divided by the annual mean emission of dust.

Fig.9 Ten year averaged Ca/Al ratio in (a) dust emission of source regions and (b) dust deposition into various ocean basins and glaciers. Elemental ratios are calculated using the annual mean emission of Ca divided by the annual mean emission of Al.

3.4 Model evaluation with observational data

The averaged modeled fractions of elements in atmospheric dust at each site for the periods for which observations are available are comparable with observations for most of the sites (Fig. 10a,b). It is clear most scatter values of model and observations are in the range of 2:1 and 1:2 line for most elements in TSP except for Mg, Mn and Si. It shows the emission inventories based on mineralogy and elemental compositions are generally consistent with the available data. A large variability in the % of different elements is observed at the 17 observational sites for most elements, especially for Ca (Fig. 10). The fraction of Fe in the fine mode particle ($PM_{2.5}$)is closer to the observational data than the TSP Fe fraction, implying that Fe in the clay soils is more accurate than that for silt. Since there are only a few reported observations of Si, this element is particularly difficult to verify. Based on averaged elemental fractions in TSP at 13 sites, the correlation coefficients (R) between modeled and observed fractions range widely (Table 3). Ca and Al had the highest correlations (0.75 and 0.72, respectively). However, the correlation coefficients for P, Mn and K were negative. For Fe, if we neglect the 3 sites in North Africa, the correlation coefficient increases from 0.29 to 0.50; in this area, the observational Fe fractions in TSP are high whereas the modeled ones are low (Fig. 10.a,5). The modeled elemental fractions in TSP are close to the observed data, with most ratios ranging between 0.7 and 1.6 (Table3).

For this comparison (above), we calculate the elemental fractions and average the fractions temporally for each site and compare to observations, but alternatively, we could average the elemental concentrations and divide by the elemental dust concentrations instead, and this will make a difference in our interpretations. For example, taking site 2-Tazhong, the averaged fraction is 3.5% when we calculate the fractions of iron firstly and average those temporally. However, when we calculate the averaged iron mass and dust mass separately, their ratio is 2.3%. For site3-Yulin, the ratio is 3.6% and 3.1% for the first method and second method, respectively. This difference maybe due to dust storm events. For this comparison, we use the first method, as we think it is more suitable for our goal of simulating the % of each element correctly.

The averaged fractions of Mg and Mn in dust are underestimated by the model at all observational sites. It should be noted that there are some uncertainities when comparing elemental fractions. When the elemental concentration is divided by particle mass concentration to obtain the elemental fraction, the errors are amplified due to error propagation associated with the combination of the error on the particle mass and that of the element concentrations. Even though the available observational data are chosen from source sites or dust events in non-source regions, the contribution from other sources could be important, especially for fine mode particles. The modeled fraction of Mn and Al in fine particles show a larger inconsistency than that those in TSP when compared with observations. Some of the discrepancies may be because the model only includes particles up to 10 μm in diameter, while the observations include larger particle fractions in TSPs. In South Asia, the elemental fractions in dust with the exception of Mn, are always much lower than at another sites, perhaps due to anthropogenic contributions to elemental particlute matter concentrations. In particular, many

metals in insoluble forms in dust particles could be from other sources such as the refractories and steel industries, construction, biomass burning or volcanic emissions (Castillo et al., 2008;Gaudichet et al., 1995; Hinkley et al., 1999; Paris et al., 2010).

The daily elemental fractions across all times and sites where there is data show that while the mean of the model was similar to the mean of the observations, there are some systematic differences (Figure 11a,b). The modeled elemental fractions are not as variable as the observations. This could be due to several issues. First there is a greater variability in the soil mineralogy and elemental composition of minerals than those included in the model (we only include the average values). Secondly, the dust model could introduce systematic errors (through advection, although this is likely to be small, as discussed in the methods section 2.1), or there could be some unaccounted anthropogenic particulate sources, modifying the dust aerosol. Also inconsistencies in the collection methods and differences in aerosol sampling periods and times could yield the observed variations in elements as concluded by Lawrence and Neff (2009).

However, the ranges of the modeled fractions of P, Ca, Fe, K and Al are close to the dominant range of the observational fractions (Fig. 11a,b). The fractions of elements in dust measured are reported to be 0.5%-2.3% for Mg, 0.065-0.2% for P, 1.0-10.2% for Ca, 0.028%-0.124% for Mn, 1.3%-7.8% for Fe, 1.2%-4.6% for K, 3.7-12.7% for Al, and 22.4%-35.7% for Si (Wilke et al. ,1984; Reheis and Kihl,1995; Stoorvogel et al., 1997; Zhang et al.,1998; Yadav and Rajamani,2004; Goudie and Middleton, 2006; Moreno et al., 2006; Jeong, 2008; Lawrence and Neff, 2009; Formenti et al., 2008; Desboeufs et al., 2010). The modeled elemental fraction in dust for P, Ca, Fe, K, Al and Si were similar to observations. However, the modeled fractions of Mg and Mn are lower (3.4 times and 3.5 times, respectively (Table 3)) than the observed ones for samples used in this study or of the above cited results. Underestimation of Mg and Mn could be due to a deficiency of minerals contaning high concentrations of Mg and Mn in our model, as dolomite (MgCO3) or palygorskyte ($(Mg,Al)_2Si_4O_{10}(OH)\cdot 4(H2O)$) are often identified in dust particles for Mg (e.g. Diaz-Hernandes et al., 2011; Kalderon et al., 2009). Moreover, it is known that the chemical composition of minerals could be variable according to the regional origin of minerals and possible impurities. For example, the Mg content in calcite ranges from 0% to 2.7% in the natural environment (Titschack et al., 2011). But in this study, the assumed fraction of Mg in calcite is zero because we took calcite as a pure mineral (see Table 1). So the underestimation of Mg in dust could be a propagation of errors in previous compositions in minerals considered in this study.

Fig.10 Comparison of observed and modeled mean fractions of elements at each site for total suspended particulates (TSP). (1-Hetian, China; 2-Tazhong, China; 3-Yu Lin, China; 4-Duolun, China; 5-Shengsi, China; 6-Hanoi, Vietnam; 7-Marnila, Philippines; 8- Balad, Iraq; 9-Baghdad, Iraq; 10-Taji,Iraq; 11-Eilat; 12-Cape Verde Island; 13-Muswellbrook, Australia; 14-Richmond, Australia, 15-Tamanrasset, Algeria; 16-Banizoumbou, Niger; 17-Douz, Tunisia). Here we calculate the elemental fractions and average the fractions temporally for each site and compare to observations.

Fig.11 Mean and quartile modeled and observational fractions of elements in (a) TSP and (b) $PM_{2.5}$ for all sites together, the box line presents 25%, 50% and 75%, individually. Here we calculate the elemental fractions and average the fractions temporally for each site and compare to observations.

Table 3 Comparison of modeled and observed fractions of elements in TSP and tuning ratio based on 14-site measurements

For reference we show the comparison of the modeled dust deposition versus observed deposition (Fig. 12). The modeled dust deposition flux agrees well with observations. The correlation coefficient between modeled and observed dust deposition is 0.86. The median of model to observation ratio is 1.15. Overall the model has been tuned to represent dust deposition, concentration and Aerosol Optical Depth (AOD) (Albani, et al., 2014), however the model has difficulty matching both deposition and concentration observations, similar to other models (Huneeus et al., 2011), suggesting more work on dust emission, transport and deposition processes is needed.

Fig.12 (a) Observational and (b) modeled dust deposition (g/m^3/year). The scale is the same for both panels. (c) A scatter plot shows the comparison between the model and observations. The correlation coefficient between observations and model results reach 0.86.

3.5 Deposition of total and soluble dust elements over the ocean, land and ice sheets

Comparisons between observations and the model simulations presented here suggest some bias in the model results (Figure 11, Table 3); subsequently the model deposition values are adjusted to better match observed measurements by the tuning ratios (Table 3; Figure 13).. Of course, improving our elemental estimates in the source region would be preferred in future studies. From the observations, we have found a wide range in fractions of elements at individual sites and at the sites together; the ratio of the maximum and minimum in measured fractions could reach more than 700 for element K, and more than 200 for Ca and Mn. Because of the limited observations, we use a global tuning factor, based on the median elemental %, and contrast this result with our default modeling approach (Table 3). It is noted that both the median of observed (3.10 %) and modeled (2.9 %) Fe was lower than 3.5%, which was thought to be the fraction of Fe in dust (e.g. Luo et al., 2008; Mahowald et al., 2008).

This study suggests significant variability in the elemental fractions in dust deposition (Figure 13, Table 4), and showed that the assumption that the fixed composition of dust being deposited over oceans is unlikely to be correct. Consistent with Mahowald et al. (2008), most dust deposition occurred downwind of dust generating regions bordering the North Atlantic, North Pacific and North Indian Ocean. The Greenland ice sheet accounted for the dominant part of elemental deposition to ice sheets regions, which is equal to the total amount of elements deposited in the whole of the South Atlantic Ocean. Fe and P are key elements in the marine ecosystem, with 6.3 Tg Fe and 184 Gg P added annually to all oceans and ice sheets (Table 5).

Table 4 Fractions (%) of elements in dust deposition into different ocean basins and ice sheets*

Also, the amounts of soluble dust element deposition are determined over different regions (see Section 2.1) (Figure 14). No atmospheric processing of natural dust or other sources of particles (e.g. anthropogenic sources) is included in this simulation. To better understand the uncertainties of soluble element deposition, estimates from two methods are used (Section 2.1) in simulating soluble elemental emission, transport and deposition. Fractional solubility of elements could not be estimated due to the lack of total element data from Method 2 (Sillanpaa (1982)). Spatial variations in fractional solubility of elements are identified by Sol-1 (mineral method) (Fig.14). Fractional solubility of Ca increases with distance from source regions because its solubility is higher in clay than in silt (Table 1b). Fractional solubility of modeled P in deposition ranges from 5% to 15%, with Saharan and Australian dust sources having solubilities averaging ~10%, consistent with Baker et al. (2006a;2006b). Previous observations suggest a fractional solubility for P of 7-100% [e.g., Graham and Duce, 1982; Chen et al., 1985; Bergametti et al., 1992; Herut et al., 1999, 2002; Ridame and Guieu, 2002]. Fractional solubility of Fe is 0.8%-1.2% in regions (Fig.14) where clay minerals such as illite play an important role (Journet et al., 2008) with a mean value of 1.17% of fractional Fe solubility (Table 1b). There is an obvious North-South gradient in the distribution of fractional solubility for Fe and Al, but with opposing magnitude (Fig.14). The fractional solubility could not be calculated using Sol-2 (Sillanpaa method) since total elemental fractions in soil were not reported in Sillanpaa (1982). Thus, the proportions of soluble Fe and K in total dust using two methods are compared with each other. This shows similar distribution patterns but the values are different (Fig. 15). The mineral method resulted in lower soluble Ca deposition and higher soluble Mg, P, Mn (Fig. 15). Our results suggest significant differences in the spatial distribution of solubility depending on which dataset is used to estimate soil solubility of elements. It should be noted that the solubility measurements by Sillanpaa (1982) were performed at different pH values (pH of 7 vs. 2) and media of extraction (acidified ultrapure waters vs. organic ligand solutions). It is known that pH and organic complexation greatly influence the fractional solubility, at least for Fe (e.g. Paris et al., 2011). Thus, that would explain the differences in elemental solubility that we computed for the dust. The soluble elemental deposition over ocean basins and ice sheets are determined using two methods and are listed in Table 5. Annual inputs of soluble Mg, P, Ca, Mn, Fe and K from mineral dust using method Sol-1 (Sol-2) were 0.28 (0.30) Tg, 16.89 (7.52) Gg, 1.32 (3.35) Tg, 22.84 (6.95) Gg, 0.068 (0.06) Tg, and 0.15 (0.25) Tg to oceans and ice sheets.

Fig.13 Percentages of elements in dust deposition（%) after tuning. It is tuned based on original percentages of elements in dust deposition in Fig. S1 by ratioing Obs./Mod. ratios listed in Table 3. Si did not change because there are not enough observational data available

Fig. 14 Fractional solubility of elements (soluble element / total element) in dust deposition (%):a. Mg, b. P, c. Ca, d. Mn, e. Fe, f. K, g. Al, h. Si

Fig. 15 Percentages of soluble elements in total dust deposition using(a) Sol-1 & (b) Sol-2 (‰), Sol-1 refer to mineral method after tuning, Sol-2 refer to Sillanpaa method described in the methods section (2).

Table 4 Deposition of dust elements into different ocean basins and glaciers

4 Summary and Conclusions

A new technique combining soil and mineralogical datasets is introduced to estimate the global emission inventory of soil associated elements Mg, P, Ca, Mn, Fe, K, Al, and Si. The spatial elemental dust emissions, transport and deposition are simulated using CESM from 2001-2010. Spatial variability of soil element fractions is characterized globally (Fig 2), and showes that the use of a constant element fraction in dust across the globe is not consistent with existing observational data for Ca and Al (Fig 10 and 11). There are few observations for elemental distributions in source regions to verify these emission, concentration and deposition simulations, but for some elements (Ca and Al), the soil elemental distribution combined with the transported dust flux in the model better captures the percentage of chemical elements in dust concentrations observed (Figure 10, 11). However, both Mg and Mn levels are underestimated by the model using the present mineral maps. The correlation of the percent of elements at different sites is not statistically significant for several elements (Mg, Mn, P and K), suggesting that improvements in the soil inventories or simulations is required, although these results could also be due to low numbers of observations. The observations and model results suggest the elemental fractions in dust varied globally and between different dust production regions, especially for Ca with values from 1% to 30%. The ratio of Ca/Al, ranged between 0.1-5.0, and is confirmed as an indicator of dust source regions (Zhang et al., 1997; Zhang et al., 2003;Sun et al., 2004a,b; Shen et al., 2007). For Fe in TSP, the median of modeled fraction is 2.90%, less than the commonly assumed 3.5% Fe used in dust models (e.g. Luo et al., 2008; Mahowald et al., 2008).

Seasonal variability of emission, concentration and deposition of most elements are simulated in the model. Also, different soluble elemental datasets show that the fractional solubility of elements varies spatially. Mineral dust element deposition fluxes into ocean basins are updated using a variable fractional elemental inventory and could have potentially important impacts on evaluating their biogeochemical effects. This study shows that soil emission inventories do a fairly good job at predicting dust elemental concentrations during dust events, except for Mg and Mn. However, the high spatial heterogeneity in elemental distributions is not captured in the model. Several sources of uncertainties exist in the model projections, the largest of which is likely to be the assumptions in the soil mappings from soil types to minerals to elemental distributions. In the future, these dust emission inventories can be combined with anthropogenic elemental inventories to further improve our understanding of elemental deposition to the oceans.

Acknowledgements

We would like to thank the US Department of Defense (DOD) for sharing chemical data from their Enhanced Particulate Matter Surveillance Program (EPMSP), and anonymous reviewers for helpful comments. We acknowledge the support of NSF grant 0932946 and1137716 and DOE-SC0006735. Simulations were conducted on the NSF National Center for Atmospheric Research's supercomputers.

Reference

Albani, S., Mahowald, N. M., Perry, A. T., Scanza, R. A., Zender, C. S., Heavens, N. G., Maggi, V., Kok, J. F., and Otto-Bliesner, B. L.: Improved dust representation in the Community Atmosphere Model, J. Adv. Model. Earth Syst., 6, 541–570, doi:10.1002/2013MS000279, 2014.

Astitha, M., Lelieveld, J., Abdel Kader, M., Pozzer, A., and de Meij, A.: Parameterization of dust emissions in the global atmospheric chemistry-climate model EMAC: impact of nudging and soil properties, Atmos. Chem. Phys., 12, 11057–11083, doi:10.5194/acp-12-11057-2012, 2012.

Baker, A. R., Kelly, S. D., Biswas, K. F., Witt, M., and Jickells, T. D.: Atmospheric deposition of nutrients to the Atlantic Ocean, Geophys. Res. Lett., 30, 2296, doi:10.1029/2003GL018518, 2003.

Baker, A. R., French, M., and Linge, K. L.: Trends in aerosol nutrient solubility along a west–east transect of the Saharan dust plume, Geophys. Res. Lett., 33, L07805, doi:10.1029/2005GL024764, 2006a.

Baker, A. R., Jickells, T. D., Witt, M., and Linge, K. L.: Trends in the solubility of iron, aluminum, manganese and phosphorus collected over the Atlantic Ocean, Mar. Chem., 98, 43–58, doi:10.1016/j.marchem.2005.06.004, 2006b.

Baker, A. R. and Croot, P. L.:. Atmospheric and marine controls on aerosol iron solubility in seawater, Mar. Chem., 120, 4–13, 2010.

Bergametti, G., Gomes, L., Coudé-Gaussen, G., Rognon, P. and Le Coustumer, M.: African dust observed over Canary Islands: Source-regions identification and transport pattern for some summer situations, J. Geophys. Res., 12, 14855–14864, doi:10.1029/JD094iD12p14855.1989.

Bergametti, G., Remoudaki, E., Losno, R., Steiner, E., Chatenet, B., and Buat-Menard, P.: Source, transport and deposition of atmospheric phosphorus over the northwestern Mediterranean, J. Atmos. Chem., 14, 501–513, doi:10.1007/BF00115254, 1992.

Boyd, P., Wong, C., Merril, J., Whitney, F., Snow, J., Harrison, P., and Gower, J.: Atmospheric iron supply and enhanced vertical carbon flux in the NE subsartic Pacific: is there a connection? Global Biogeochem. Cy., 12, 429–441, 1998.

Buck, C., Landing, W. M., Resing, J. A., and Lebon, G.: Aerosol iron and alumninum solubility in the northwest Pacific Ocean: results from the 2002 IOC Cruise, Geochem. Geophy. Geosy., 7, Q04M07, doi:10.1029/2005GC000977, 2006.

Capone, D. G., Zehr, J. P., Paerl, H. W., Bergman, B., and Carpenter, E. J.: Trichodesmium, a globally significant marine cyanobacterium, Science, 276, 1221–1229, 1997.

Carpenter, L. J., Fleming, Z. L., Read, K. A., Lee, J. D., Moller, S. J., Hopkins, J. R., Purvis, R. M., Lewis, A. C., Müller, K., Heinold, B., Herrmann ,H., Fomba, K. W., Pinxteren, D. v., Müller, C., Tegen, I., Wiedensohler, A., Müller, T., N. Niedermeier, Achterberg, E. P., Patey, M. D., Kozlova, E. A., Heimann, M., Heard, D. E., Plane, J. M. C., Mahajan, A., Oetjen, H., Ingham, T., Stone, D., Whalley, L. K., Evans, M. J., Pilling, M. J., Leigh, R. J., Monks, P. S., Karunaharan, A., Vaughan, S., Arnold, S. R., Tschritter, J., Pöhler, D., Frieß, U., Holla, R., Mendes, L. M., Lopez, H., Faria, B., Manning, A. J., and Wallace, D. W. R.: Seasonal characteristics of tropical marine boundary layer air measured at the Cape Verde Atmospheric Observatory, J. Atmos. Chem., 67, 87–140, doi:10.1007/s10874-011-9206-1, 2010.

Castillo, S., Moreno, T., Querol, X., Alastuey, A., Cuevas, E., Herrmann, L., Monkaila, M., and Gibbons, W.: Trace element variation in size-fractionated African desert dusts, J. Arid Environ. 72, 1034–1045, 2008.

Chen, L. , Arimoto R., and Duce R. A.: The sources and forms of phosphorus in marine aerosol particles and rain from Northern New Zealand, Atmos. Environ., 19, 779–787, 1985.

613 Chen, H.-Y., Fang, T.-H., Preston, M., and Lin, S.: Characterization of phosphorus in the aerosol of a coastal
614 atmosphere: using as equential extraction method, Atmos. Environ., 40, 279–289,
615 doi:10.1016/j.atmosenv.2005.09.051, 2006.

616 Chen, Y. and Siefert, R.: Sesaonal and spatial distributions and dry deposition fluxes of atmospheric total and labile
617 iron over the tropical and subtropical North Atlantic Ocean, J. Geophys. Res., 109, D09305,
618 doi:10.1029/2003JD003958, 2004.

619 Chen, Y., Paytan, A., Chase, Z., Measures, C., Beck, A. J., Sañudo-Wilhelmy, S. A., and Post, A. F.: Sources and
620 fluxes of atmospheric trace elements to the Gulf of Aqaba, Red Sea, J. Geophys. Res., 113, D05306,
621 doi:10.1029/2007JD009110, 2008.

622 Claquin, T., Schulz, M., and Balkanski, Y. J.: Modeling the mineralogy of atmospheric dust sources, J. Geophys.
623 Res., 104, 22243–22256, 1999.

624 Cohen, D. D., Stelcer, E., Hawas, O., and Garton, D.: IBA methods for characterisation of fine particulate
625 atmospheric pollution: a local, regional and global research problem, Nucl. Instrum. Meth. B, 219, 145–152, 2004.

626 Cohen, D. D., Stelcer, E., Garton, D., and Crawford, J.: Fine particle characterization, source apportionment and
627 long range dust transport into the Sydney Basin: a long term study between

628 1998 and 2009, Atmospheric Pollution Research, 2, 182–189, 2011.

629 Desboeufs, K., Journet, E., Rajot, J.-L., Chevaillier, S., Triquet, S., Formenti, P., and Zakou, A.: Chemistry of rain
630 events inWest Africa: evidence of dust and biogenic influence in convective systems, Atmos. Chem. Phys., 10,
631 9283–9293, doi:10.5194/acp-10-9283-2010, 2010.

632 Duce, R. A. and Tindale, N. W.: Atmospheric transport of iron and its deposition in the ocean, Limnol. Oceanogr.,
633 36, 1715–1726, 1991.

634 Christian, J.R. Advection in plankton models with variable elemental ratios. Ocean Dynamics, 57(1), 63-71.
635 doi:10.1007/s10236-006-0097-7, 2007.

636 Duce, R. A., Liss, P. S., Merrill, J. T., Atlas, E. L., Buat-Me ard, P., Hicks, B. B., Miller, J. M., Prospero, J. M.,
637 Arimoto, R., Church, T. M., Ellis, W., Galloway, J. N., Hansen, L., Jickels, T. D., Knap, A. H., Reinhardt, K. H.,
638 Schneider, B., Soudine, A., Tokos, J. J., Tsunogai, S., Wollast, R., and Zhou, M.: The atmospheric input of trace
639 species to the world ocean, Global Biogeo chem. Cy., 5, 193–259, 1991.

640 Engelbrecht, J., McDonald, E., Gillies, J., Jayanty, R. K. M., Casuccio, G., and Gertler, A. W.: Characterizing
641 mineral dusts and other aerosols from the Middle East – Part 1: Ambient sampling, Inhal. Toxicol., 21, 297–326,
642 2009.

643 Engelbrecht, J. P., Menendez, I., and Derbyshire, E.: Sources of $PM_{2.5}$ impacting on Gran$_5$ Canaria, Spain, Catena,
644 117, 119–132, doi:10.1016/j.catena.2013.06.017, 2014.

645 FAO-Unesco: Soil Map of the World, Southeast Asia, 1976, Sheet IX, Edition I, 1976.

646 Formenti, P., Rajot, J. L., Desboeufs, K., Caquineau, S., Chevaillier, S., Nava, S., Gaudichet, A., Journet, E., Triquet,
647 S., Alfaro, S., Chiari, M., Haywood, J., Coe, H., and Highwood, E.: Regional variability of the composition of
648 mineral dust from western Africa: results from the AMMA SOP0/DABEX and DODO field campaigns, J. Geophys.
649 Res., 113, D00C13,

650 doi:10.1029/2008JD009903, 2008.

651 Formenti, P., Schütz, L., Balkanski, Y., Desboeufs, K., Ebert, M., Kandler, K., Petzold, A., Scheuvens, D.,
652 Weinbruch, S., and Zhang, D.: Recent progress in understanding physical and chemical properties of African and
653 Asian mineral dust, Atmos. Chem. Phys., 11, 8231–8256, doi:10.5194/acp-11-8231-2011, 2011.

Fung, I., Meyn, S. K., Tegen, I., Doney, S., John, J., and Bishop, J.: Iron supply and demand in the upper ocean, Global Biogeochem. Cy., 14, 281–295, 2000.

Gaudichet, A., Echalar, F., Chatenet, B., Quisefit, J. P., Malingre, G., Cachier, H., Buatmenard, P., Artaxo, P., and Maenhaut, W.: Trace elements in tropical African savanna biomass burning aerosols, J. Atmos. Chem., 22, 19–39, 1995.

Gold, C. M., Cavell, P. A., and Smith, D. G. W.: Clay minerals in mixtures: sample preparation, analysis, and statistical interpretation, Clay. Clay Miner., 3, 191–199, 1983.

Goudie, A. S. and Middleton, N. J.: Desert Dust in the Global System, Springer, Berlin, 2006.

Graham, W. F. and Duce, R. A.: The atmospheric transport of phosphorus to the western North Atlantic, Atmos. Environ., 16, 1089–1097, doi:10.1016/0004-6981(82)90198-6, 1982.

Guieu, C., Bonnet, S., Wagener, T., and Loye-Pilot, M.-D.: Biomass burning as a source of dissolved iron to the open ocean?, Geophys. Res. Lett., 22, L19608, doi:10.1029/2005GL022962, 2005.

Guo, L., Chen, Y., Wang, F. J., Meng, X., Xu, Z. F., and Zhuang, G.: E_ ects of Asian dust on the atmospheric input of trace elements to the East China Sea, Mar. Chem., 163, 19–27, doi:10.1016/j.marchem.2014.04.003, 2014.

Hand, J. L., Mahowald, N. M., Chen, Y., Siefert, R. L., Luo, C., Subramaniam, A., and Fung, I.: Estimates of atmospheric-processed soluble iron from observations and a global mineral aerosol model: Biogeochemical implications, J. Geophys. Res., 109, D17205, doi:10.1029/2004JD004574, 2004.

Herut, B., Krom, M., Pan, G., and Mortimer, R.: Atmospheric input of nitrogen and phosphorus to the southeast Mediterranean: sources, fluxes and possible impact, Limnol. Oceanogr., 44, 1683–1692, 1999.

Herut, B., Collier, R., and Krom, M.: The role of dust in supplying nitrogen and phosphorus to the southeast Mediterranean, Limnol. Oceanogr., 47, 870–878, 2002.

Herut, B., Zohary, T., Krom, M. D., Mantoura, R. F. C., Pitta, V., Psarra, S., Rassoulzadegan, F., Tanaka, T., and Thingstad, F. T.: Response of east Mediterranean surface water to Saharan dust: on-board microcosm experiment and field observations, Deep-Sea Res. Pt. II, 52, 3024–3040, doi:10.1016/j.dsr2.2005.09.003, 2005.

Hinkley, T. K., Lamothe, P. J., Wilson, S. A., Finnegan, D. L., and Gerlach, T. M.: Metal emissions from Kilauea, and a suggested revision of the estimated worldwide metal output by quiescent degassing of volcanoes, Earth Planet. Sc. Lett., 170, 315–325, 1999.

Huneeus, N., Schulz, M., Balkanski, Y., Griesfeller, J., Prospero, J., Kinne, S., Bauer, S., Boucher, O., Chin, M., Dentener, F., Diehl, T., Easter, R., Fillmore, D., Ghan, S., Ginoux, P., Grini, A., Horowitz, L., Koch, D., Krol, M. C., Landing, W., Liu, X., Mahowald, N., Miller, R., Morcrette, J.-J., Myhre, G., Penner, J., Perlwitz, J., Stier, P., Takemura, T., and Zender, C. S.: Global dust model intercomparison in AeroCom phase I, Atmos. Chem. Phys., 11, 7781–7816, doi:10.5194/acp-11-7781-2011, 2011.

Jeong, G. Y.: Bulk and single-particle mineralogy of Asian dust and a comparison with its source soils, J. Geophys. Res., 113, D02208, doi:10.1029/2007jd008606, 2008.

Jickells, T., An, Z., Andersen, K., Baker, A., Bergametti, G., Brooks, N., Cao, J., Boyd, P., Duce, R., Hunter, K., Kawahata, H., Kubilay, N., LaRoche, J., Liss, P., Mahowald, N., Prospero, J., Ridgwell, A., Tegen, I., and Torres, R.: Global iron connections between dust, ocean biogeochemistry and climate, Science, 308, 67–71, 2005.

Journet, E., Desboeufs, K. V., Caquineau, S., and Colin, J.-L.: Mineralogy as a critical factor of dust iron solubility, Geophys. Res. Lett., 35, L07805, doi:10.1029/2007gl031589, 2008.

Journet, E., Balkanski, Y., and Harrison, S. P.: A new data set of soil mineralogy for dust-cycle modeling, Atmos. Chem. Phys., 14, 3801–3816, doi:10.5194/acp-14-3801-2014, 2014.

695 Kandler, K., Benker, N., Bundke, U., Cuevas, E., Ebert, M., Knippertz, P., Rodríguez, S., Schütz, L., and
696 Weinbruch, S.: Chemical composition and complex refractive index of Saha- ran mineral dust at Izaña, Tenerife
697 (Spain) derived by electron microscopy, Atmos. Environ., 41, 8058–8074, 2007.

698 Kok, J. F.: A scaling theory for the size distribution of emitted dust aerosols suggests climate models underestimate
699 the size of the global dust cycle, P. Natl. Acad. Sci. USA, 108, 1016–021, 2011.

700 Kreutz, K. J. and Sholkovitz, E. R.: Major element, rare earth element, and sulfur isotopic composition of a high-
701 elevation firncore: sources and transport of mineral dust in central Asia, Geochem. Geophy. Geosy., 1, 1048–1071,
702 2000.

703 Lam, P. and Bishop, J.: The continental margin is a key sources of iron to the North Pacific Ocean, Geophys. Res.
704 Lett., 35, L07608, doi:10.1029/2008GL033294, 2008.

705 Lawrence, C. R. and Ne, J. C.: The physical and chemical flux of eolian dust across the landscape: a synthesis of
706 observations and an evaluation of spatial patterns, Chem. Geol., 267, 46–63, doi:10.1016/j.chemgeo.2009.02.005,
707 2009.

708 Li, G., Chen, J., Chen, Y., Yang, J., Ji, J., and Liu, L.: Dolomite as a tracer for the source regions of Asian dust, J.
709 Geophys. Res., 112, D17201, doi:10.1029/2007jd008676, 2007.

710 Lin, S.-J., and R. B. Rood. An explicit flux-form semi-Lagrangian shallow-water model on the sphere, Quarterly
711 Journal of the Royal Meteorological Society, 123, 2477-2498,1997.

712 Luo, C., Mahowald, N., Bond, T., Chuang, P. Y., Artaxo, P., Siefert, R., Chen, Y., and Schauer, J.: Combustion
713 irondistribution and deposition, Global Biogeochem. Cy., 22, GB1012, doi:10.1029/2007GB002964, 2008.

714 Mahowald, N.; Baker, A.; Bergametti, G.; Brooks, N.; Duce, R.; Jickells, T.; Kubilay, N.; Prospero, J.; Tegen, I.
715 Atmospheric global dust cycle and iron inputs to the ocean, Global Biogeochem. Cy., 19, GB4025,
716 doi:10.1029/2004GB002402, 2005.

717 Mahowald, N., Muhs, D. R., Levis, S., Rasch, P. J., Yoshioka, M., Zender, C. S., and Luo, C.: Change in
718 atmospheric mineral aerosols in response to climate: last glacial period, preindustrial, modern, and doubled carbon
719 dioxide climates, J. Geophys. Res.-Atmos., 111, D10202, doi:10.1029/2005JD006653, 2006.

720 Mahowald, N., Jickells, T. D., Baker, A. R., Artaxo, P., Benitez-Nelson, C. R., Bergametti, G., Bond, T. C., Chen,
721 Y., Cohen, D. D., Herut, B., Kubilay, N., Losno, R., Luo, C., Maenhaut, W., McGee, K. A., Okin, G. S., Siefert, R.
722 L., and Tsukuda, S.: Global distribution of atmospheric phosphorus sources, concentrations and deposition rates, and
723 anthropogenic impacts, Global Biogeochem. Cy., 22, GB4026, doi:10.1029/2008GB003240, 2008.

724 Marino, F., Maggi, V., Delmonte, B., Ghermandi, G., and Petit, J. R.: Elemental composition (Si, Fe, Ti) of
725 atmosphericdust over the last 220 kyr from the EPICA ice core (Dome C, Antarctica), Ann. Glaciol., 39, 110–118,
726 doi:10.3189/172756404781813862, 2004.

727 Marteel, A., Gaspari, V., Boutron, C. F., Barbante, C., Gabrielli, P., Cescon, P., Ferrari, C., Dommergue, A.,
728 Rosman, K., Hong, S., and Hur, S.: Climate-related variations in crustal trace elements in Dome C (East Antarctica)
729 ice during the past 672 kyr, Climatic Change, 92, 191–211, 2009.

730 Martin, J. H., Gordon, R. M., and Fitzwater, S. E.: The case for iron, Limnol. Oceanogr., 36, 1793–1802, 1991.

731 Measures, C. and Vink, S.: On the use of dissolved aluminum in surface waters to estimate dust deposition to the
732 ocean, Global Biogeochem. Cy., 14, 317–327, 2000.

733 Mermut, A. R. and Cano, A. F.: Baseline studies of the clay minerals society source clays: chemical analyses of
734 major elements, Clay. Clay Miner., 49, 381–386, 2001.

735 Mills, M. M., Ridame, C., Davey, M., LaRoche, J., and Geider, R.: Iron and phosphorus co-limit nitrogen fixation in

the eastern tropical North Atlantic, Nature, 429, 292–294, 2004.

Moore, J. K. and Braucher, O.: Sedimentary and mineral dust sources of dissolved iron to the world ocean, Biogeosciences, 5, 631–656, doi:10.5194/bg-5-631-2008, 2008.

Morel, F. M. M., Milligan, A. J., and Saito, M. A.: Marine bioinorganic chemistry: the role of trace metals in the oceanic cycles of major nutrients, in: Treatise on Geochemistry, Vol. 6., Elsevier, Pergamon, Oxford, 113–143, ISBN 0-08-043751-6, 2003.

Moreno, T., Querol, X., Castillo, S., Alastuey, A., Cuevas, E., Herrmann, L., Mounkaila, M., Elvira, J., and Gibbons, W.: Geochemical variations in aeolian mineral particles from the Sahara-Sahel dust corridor, Chemosphere, 65, 261–270, 2006.

Nickovic, S., Vukovic, A., Vujadinovic, M., Djurdjevic, V., and Pejanovic, G.: Technical Note: High-resolution mineralogical database of dust-productive soils for atmospheric dust modeling, Atmos. Chem. Phys., 12, 845–855, doi:10.5194/acp-12-845-2012, 2012.

Nickovic S., Vukovic A., Vujadinovic M. (2013). Atmospheric processing of iron carried by mineral dust. Atmos. Chem. Phys., 13,9169–9181, doi:10.5194/acp-13-9169-2013, 2013.

Nozaki, Y.: A fresh look at element distribution in the North Pacific, EOS T. Am. Geophys. Un.,78, 221–221, doi:10.1029/97EO00148, 1997.

Okin, G. S., Mahowald, N., Chadwick, O. A., and Artaxo, P.: Impact of desert dust on the biogeochemistry

Of phosphorus in terrestrial eco-systems, Global Biogeochem. Cy., 18, GB2005, doi:10.1029/2003GB002145, 2004.

Paris, R., Desboeufs, K. V., Formenti, P., Nava, S., and Chou, C.: Chemical characterization of iron in dust and biomass burning aerosols during AMMA-SOP0/DABEX: implication for iron solubility, Atmos. Chem. Phys., 10, 4273–4282, doi:10.5194/acp-10-4273-2010, 2010.

Paytan, A., Mackey, K., Chen, Y., Lima, I., Doney, S., Mahowald, N., Lablosa, R., and Post, A.: Toxicity of atmospheric aerosols on marine phytoplankton, P. Natl. Acad. Sci. USA, 106, 106, 4601–4605, doi:10.1073/pnas.0811486106, 2009.

Perry, K. D., Cahill, T. A., Eldred, R. A., Dutcher, D. D., and Gill, T. E.: Long-range transport of North African dust to the eastern United States, J. Geophys. Res.-Atmos., 102, 11225–11238, 1997.

Petrucci, R. H., Harwood, W. S., Herring, G., Madura, J.: General Chemistry: Principles and Modern Application, 9th edn., Printice Hall, New Jersey, Pearson2001.

Prospero, J. M., Landing, W. M., and Schulz, M.: African dust deposition to Florida: temporal and spatial variability and comparisons to models, J. Geophys. Res., 115, D13304,doi:10.1029/2009JD012773, 2010.

Rasch, P., D. Coleman, N. Mahowald, D. Williamson, S.-J. Lin, B. Boville, and P. Hess. Characteristics of atmospheric transport using three numerical formulations for atmospheric dynamics in a single GCM framework, Journal of Climate, 19, 2243-2266, 2006.

Reheis, M. C. and Kihl, R.: Dust deposition in southern Nevada and California, 1984–1989 –relations to climate, source area, and source lithology, J. Geophys. Res.-Atmos., 100, 8893–8918, 1995.

Reid, E. A., Reid, J. S., Meier, M. M., Dunlap, M. R., Cli_ , S. S., Broumas, A., Perry, K., and Maring, H.: Characterization of African dust transported to Puerto Rico by individual particle and size segregated bulk analysis, J. Geophys. Res., 108, 8591, doi:10.1029/2002JD002935, 2003.

Ridame, C. and Guieu, C.: Saharan input of phosphate to the oligotrophic water of the open western Mediterranean

776 Sea, Limnol. Oceanogr., 47, 856–869, 2002.

777 Scanza, R. A., Mahowald, N., Ghan, S., Zender, C. S., Kok, J. F., Liu, X., and Zhang, Y.: Modeling dust as
778 component minerals in the Community Atmosphere Model: development of framework and impact on radiative
779 forcing, Atmos. Chem. Phys. 15, 537-561, 2015.

780 Schütz, L. and Rahn, K. A.: Trace element concentrations in erodible soils, Atmos. Environ., 16, 171–176, 1982.

781 Seinfeld, J. H. and Pandis, S. N.: Atmospheric Chemistry and Physics: from Air Pollution to Climate Change, J.
782 Wiley, New York, 1998.

783 Shao, Y.: A model for mineral dust emission, J. Geophys. Res., 106, 20239–20254, doi:10.1029/2001jd900171,
784 2001.

785 Shen, Z. X., Li, X., Cao, J., Caquineau, S., Wang, Y., and Zhang, X.: Characteristics of clay minerals in Asian dust
786 and their environmental significance, China Part., 3, 260–264, 2005.

787 Shen, Z. X., Cao, J., Li, X., Okuda, T., Wang, Y., and Zhang, X.: Mass concentration and mineralogical
788 characteristics of aerosolparticles collected at Dunhuang during ACE-Asia, Adv. Atmos. Sci., 23, 291–298, 2006.

789 Shen, Z. X., Cao, J. J., Arimoto, R., Zhang, R. J., Jie, D. M., Liu, S. X., Zhu, C.S.: Chemical composition and
790 source characterization of spring aerosol over Horqin sand land in northeastern China, J. Geophys. Res., 112,
791 D14315, doi:10.1029/2006JD007991, 2007.

792 Sillanpää, M.: Micronutrients and the Nutrient Status of Soils: a Global Study, FAO Soils Bulletin, No. 48.,
793 Appendix 6–7, Rome, 1982.

794 Stoorvogel, J. J., VanBreemen, N., and Janssen, B. H.: The nutrient input by Harmattan dust to a forest ecosystem in
795 Côte d'Ivoire, Africa, Biogeochemistry, 37, 145–157, 1997.

796 Sun, Y., Zhuang, G., Yuan, H., Zhang, X., and Guo, J.: Characteristics and sources of 2002 super dust storm in
797 Beijing, Chinese Sci. Bull., 49, 698–705, 2004a.

798 Sun, Y., Zhuang, G., Wang, Y., Han, L., Guo, J., Dan, M., Zhang, W., Wang, Z., and Hao, Z.: The air-borne
799 particulate pollution in Beijing – concentration, composition, distribution and sources, Atmos. Environ., 38, 5991–
800 6004, 2004b.

801 Svensson, A., Biscaye, P. E., and Grousset, F. E.: Characterizationof late glacial continental dust in the Greenland
802 Ice Core Project ice core, J. Geophys. Res., 105, 4637–4656, doi:10.1029/1999jd901093, 2000.

803 Swap, R., Garstang, M., Greco, S., Talbot, R., and Kallberg, P.: Saharan dust in the Amazon Basin, Tellus B, 44,
804 133–149, 1992.

805 Textor, C., Schulz, M., Guibert, S., Kinne, S., Balkanski, Y., Bauer, S., Berntsen, T., Berglen, T., Boucher, O., Chin,
806 M., Dentener, F., Diehl, T., Easter, R., Feichter, H., Fillmore, D., Ghan, S., Ginoux, P., Gong, S., Grini, A.,
807 Hendricks, J., Horowitz, L., Huang, P., Isaksen, I., Iversen, I., Kloster, S., Koch, D., Kirkevåg, A., Kristjansson, J. E.,
808 Krol, M., Lauer, A., Lamarque, J. F., Liu, X., Montanaro, V., Myhre, G., Penner, J., Pitari, G., Reddy, S., Seland, Ø.,
809 Stier, P., Takemura, T., and Tie, X.: Analysis and quantification of the diversities of aerosol life cycles within
810 AeroCom, Atmos. Chem. Phys., 6, 1777–1813, doi:10.5194/acp-6-1777-2006, 2006.

811 Textor, C., Schulz, M., Guibert, S., Kinne, S., Balkanski, Y., Bauer, S., Berntsen, T., Berglen, T., Boucher, O., Chin,
812 M., Dentener, F., Diehl, T., Feichter, J., Fillmore, D., Ginoux, P., Gong, S., 30 Grini, A., Hendricks, J., Horowitz, L.,
813 Huang, P., Isaksen, I. S. A., Iversen, T., Kloster, S., Koch, D., Kirkevåg, A., Kristjansson, J. E., Krol, M., Lauer, A.,
814 Lamarque, J. F., Liu, X., Montanaro, V., Myhre, G., Penner, J. E., Pitari, G., Reddy, M. S., Seland, Ø., Stier, P.,
815 Takemura, T., and Tie, X.: The e_ ect of harmonized emissions on aerosol properties in global models – an
816 AeroCom experiment, Atmos. Chem. Phys., 7, 4489–4501, doi:10.5194/acp-7-4489-2007, 2007.

817 Titschack, J., Goetz-Neunhoe_ er, F., and Neubauer, J.: Magnesium quantification in calcites [(Ca,Mg)CO_3] by
818 Rietveld-based XRD analysis: revisiting a well-established method, Am. 5 Mineral., 96, 1028–1038, 2011.

819 Wang, Q., Zhuang, G., Li, J., Huang, K., Zhang, R., Jiang, Y., Lin, Y., and Fu, J. S.: Mixing of dust with pollution
820 on the transport path of Asian dust – revealed from the aerosol over Yulin, the north edge of Loess Plateau, Sci.
821 Total Environ., 409, 573–581, 2010.

822 Werner, M., Tegen, I., Harrison, S. P., Kohfeld, K. E., Prentice, I. C., Balkanski, Y., Rodhe, H., and Roelandt., C.:
823 Seasonal and interannual variability of the mineral dust cycle under present and glacial climate conditions, J.
824 Geophys. Res., 107, D244744, doi:10.1029/2002JD002365, 2002.

825 Wilke, B. M., Duke, B. J., and Jimoh, W. L. O.: Mineralogy and chemistry of Harmattan dust in northern Nigeria,
826 Catena, 11, 91–96, 1984.

827 Xuan, J., Sokolik, I. N., Hao, J., Guo, F., Mao, H., and Yang, G.: Identification and characterization of sources of
828 atmospheric mineral dust in East Asia, Atmos. Environ., 38, 6239–6252, 2004.

829 Yadav, S. and Rajamani, V.: Geochemistry of aerosols of northwestern part of India adjoining the Thar Desert,
830 Geochim. Cosmochim. Ac., 68, 1975–1988, 2004.

831 Zender, C., Bian, H., and Newman, D.: Mineral Dust Entrainment and Deposition (DEAD) model: description and
832 1990s dust climatology, J. Geophys. Res., 108, 4416, doi:10.1029/2002JD002775, 2003.

833 Zhang, X. Y., Arimoto, R., and An, Z. S.: Dust emission from Chinese desert sources linked to variation in
834 atmospheric circulation, J. Geophys. Res., 102, 28041–28047, 1997.

835 Zhang, X. Y., Arimoto, R., Zhu, G. H., Chen, T., and Zhang, G. Y.: Concentration, size distribution and deposition
836 of mineral aerosol over Chinese desert regions, Tellus B, 50, 317–330, 1998.

837 Zhang, X. Y., Gong, S. L., Shen, Z. X., Mei, F. M., Xi, X. X., Liu, L. C., Zhou, Z. J., Wang, D., Wang, Y. Q., and
838 Cheng, Y.: Characterization of soil dust aerosol in China and its transport and distribution during 2001 ACE-Asia: 1.
839 Network observations, J. Geophys. Res., 108, 4261, doi:10.1029/2002jd002632, 2003.

840

841

Main Tables 1- 5

Table1a Generalized mineral compositions (%) applied in this study

Table1b Elemental solubility as a percentage of the element contained in the minerals (%)

Table 2 Ten year averaged emission rates (Tg/yr) and percentages of elements over desert regions (%)

Table 3 Comparison of modeled and observed fractions of chemical elements in TSP and tuning ratio based on 14-site measurements

Table 4 Fractions (%) of elements in dust deposition into different ocean basins and ice sheets*

Table 5 Deposition of dust elements into different oceans and ice sheets*

855 **Table1a Generalized mineral compositions (%) applied in this study**

Mineral	Mg	P	Ca	Mn	Fe	Al	Si	K
Smectite	1.21	0.17	0.91	0.03	2.55	8.57	27.44	0.27
Illite	0.85	0.09	1.45	0.03	4.01	10.47	24.11	4.28
Hematite	0.09	0.18	0.12	0.07	57.50	2.67	2.11	0.07
Feldspar	0.15	0.09	3.84	0.01	0.34	10.96	25.24	5.08
Kaolinite	0.02	0.16	0.03	0.01	0.24	20.42	20.27	0.00
Calcite	0.00	0.00	40.00	0.00	0.00	0.00	0.00	0.00
Quartz	0.00	0.00	0.00	0.00	0.00	0.00	46.70	0.00
Gypsum	0.00	0.00	23.30	0.00	0.00	0.00	0.00	0.00

856

857 **Table1b Elemental solubility as a percentage of the element contained in the minerals (%)**

Mineral	Mg	P	Ca	Mn	Fe	Al	Si	K
Smectite	14.09	2.93	79.20	25.35	2.60	0.00	0.05	31.41
Illite	7.80	30.58	50.96	24.93	1.17	0.15	0.05	2.87
Hematite	0.00	0.00	0.00	3.39	0.01	0.00	0.00	0.00
Feldspar	5.17	0.00	4.46	4.71	3.01	0.12	0.02	4.53
Kaolinite	22.32	0.00	21.97	0.00	4.26	0.38	0.37	0.00
Calcite	0.00	0.00	7.00	0.00	0.00	0.00	0.00	0.00
Quartz	0.00	0.00	0.00	0.00	0.00	0.00	0.0003	0.00
Gypsum	0.00	0.00	0.56	0.00	0.00	0.00	0.00	0.00

858

859 *Fe content came from Journet et al. (2008), the other elements were from personal communication with E. Journet.

860

861

862

Table 2 Ten year averaged emission rates (Tg/yr) and percentages of elements over desert regions (%)

(For this table, annual mean emission of each element is divided by the annual mean emission of dust to obtain the %.)

Source Regions	**Mg**	**P**	**Ca**	**Mn**	**Fe**	**K**	**Al**	**Si**	**Dust**
WAsia	0.91	1.77E-01	12.73	3.53E-02	5.53	3.70	16.71	72.43	251.17
NCAsia	0.50	9.27E-02	6.05	1.80E-02	2.26	1.90	8.36	37.99	128.59
CAsia	0.13	2.54E-02	1.57	4.98E-03	0.70	0.55	2.35	9.77	33.82
SCAsia	0.05	1.07E-02	0.54	1.93E-03	0.29	0.22	1.04	4.07	13.91
EAsia	0.21	4.38E-02	1.62	8.16E-03	1.28	0.85	4.22	18.27	58.90
Asian Region	**1.79**	**3.50E-01**	**22.52**	**6.84E-02**	**10.06**	**7.23**	**32.67**	**142.54**	**486.4**
ESah	1.23	2.74E-01	11.98	4.83E-02	6.62	5.41	26.45	102.59	346.16
WSah	2.62	5.31E-01	30.67	1.01E-01	14.25	11.04	50.35	208.70	712.00
SNAf	0.02	1.17E-02	0.17	1.47E-03	0.37	0.12	1.25	4.33	13.98
SAf	0.01	3.10E-03	0.18	5.90E-04	0.11	0.06	0.31	1.34	4.46
Africa	3.89	8.20E-01	42.99	1.51E-01	21.34	16.63	78.36	316.96	1076.6
NWNAm	0.00002	4.70E-06	0.0001	8.00E-07	0.0002	0.0001	0.0005	0.0019	0.030
SWNAm	0.02	3.01E-03	0.16	6.00E-04	0.10	0.07	0.29	1.27	4.20
North America	**0.02**	**3.02E-03**	**0.16**	**6.00E-04**	**0.10**	**0.07**	**0.29**	**1.27**	**4.2**
SAm	0.0005	1.20E-04	0.01	2.00E-05	0.003	0.002	0.01	0.04	0.15
Patag	0.03	6.79E-03	0.27	1.32E-03	0.20	0.13	0.62	2.82	9.08
South America	**0.03**	**6.91E-03**	**0.27**	**1.34E-03**	**0.21**	**0.13**	**0.63**	**2.86**	**9.2**
WAstr	0.0005	1.30E-04	0.003	2.00E-05	0.003	0.002	0.01	0.05	0.16
EAstr	0.02	5.13E-03	0.20	9.10E-04	0.16	0.10	0.48	1.78	6.11
Australia region	**0.02**	**5.26E-03**	**0.20**	**9.30E-04**	**0.17**	**0.10**	**0.49**	**1.83**	**6.3**
Global	**5.75**	**1.18E+00**	**66.14**	**2.22E-01**	**31.87**	**24.15**	**112.44**	**465.46**	**1582.7**
Global mean % element	**0.36**	**0.07**	**4.18**	**0.01**	**2.01**	**1.53**	**7.10**	**29.41**	**/**
Min. % element in 15 SR*	0.17	0.07	1.19	0.01	1.67	0.86	6.50	28.84	/
Max. % element in 15 SR*	0.39	0.08	5.07	0.02	2.68	1.63	8.96	31.38	/

*SR refer to source regions

Table 3 Comparison of modeled and observed fractions of chemical elements in TSP, and tuning ratio based on 13-site measurements. (For this table comparing the elemental ratios at the measurement sites, the % value at each time measured is averaged across time and space for this comparison.)

	Mg	P	Ca	Mn	Fe	K	Al
Corr. coeff. Of Averaged Fractions	0.14	-0.32	0.75	-0.51	0.29	-0.16	0.72
Median of Obs. (%)	1.45	0.09	5.42	0.070	3.10	1.79	5.26
Median of Mod.(%)	0.43	0.08	3.41	0.020	2.29	1.54	7.81
Obs./Mod. Median Ratio (tuned ratio)	3.4	1.1	1.6	3.5	1.4	1.2	0.7

Table 4 Fractions (%) of elements in dust deposition into different ocean basins and ice sheets*

Ocean Basins/Glacier	Mg	P	Ca	Mn	Fe	K	Al	Si**
North Atlantic	1.43	0.10	5.36	0.06	3.05	1.89	5.96	28.32
South Atlantic	1.50	0.10	5.36	0.06	3.35	1.84	6.01	28.07
North Pacific	1.56	0.10	5.92	0.06	3.26	1.90	5.78	28.01
South Pacific	1.47	0.10	5.30	0.06	3.87	1.86	6.15	27.61
North Indian	1.38	0.08	7.90	0.05	3.13	1.81	4.95	28.29
South Indian	1.53	0.10	6.50	0.06	3.64	1.87	5.88	27.33
Southern Ocean	1.56	0.10	5.12	0.06	3.74	1.88	5.88	28.25
Arctic	1.60	0.10	6.23	0.06	3.31	1.96	5.76	27.76
Mediterranean	1.37	0.08	7.14	0.05	2.90	1.88	4.85	29.14
Antarctic ice sheets	1.50	0.10	4.90	0.06	3.54	1.82	5.55	29.17
Greenland ice sheets	1.50	0.09	7.49	0.06	2.82	1.89	5.24	28.00
Averaged	1.49	0.10	6.11	0.06	3.33	1.87	5.64	28.18

*After timing tuned ratios (Table 3) except for Si

** Not tuning

(For this table, annual mean deposition of each element is divided by the annual mean deposition of dust to obtain the %.)

883 **Table 5 Deposition of dust elements into different oceans and ice sheets***

Ocean / ice sheet	Mg (Tg/yr)			P (Gg/yr)			Ca (Tg/yr)			Mn (Gg/yr)			Fe (Tg/yr)			K (Tg/yr)		
	Total	Sol-1	Sol-2	**Total**	Sol-1	Sol-2	**Total**	Sol-1	Sol-2	**Total**	Sol-1	Sol-2	**Total**	Sol-1	Sol-2	**Total**	Sol-1	Sol-2
North Atlantic	**1.50**	0.16	0.14	**103.12**	8.81	4.10	**5.64**	0.68	1.81	**58.90**	12.08	3.87	**3.20**	0.036	0.033	**1.99**	0.008	0.136
South Atlantic	**0.13**	0.01	0.02	**8.84**	0.79	0.38	**0.47**	0.06	0.17	**5.17**	1.07	0.34	**0.30**	0.003	0.003	**0.16**	0.007	0.014
North Pacific	**0.28**	0.03	0.03	**17.47**	1.66	0.65	**1.06**	0.13	0.33	**10.58**	2.25	0.58	**0.58**	0.007	0.006	**0.34**	0.014	0.025
South Pacific	**0.01**	0.001	0.001	**0.86**	0.07	0.04	**0.04**	0.006	0.01	**0.50**	0.10	0.03	**0.03**	0.0003	0.000	**0.02**	0.0007	0.001
North Indian	**0.56**	0.06	0.06	**34.38**	3.54	1.52	**3.23**	0.29	0.63	**21.86**	4.62	1.35	**1.28**	0.013	0.013	**0.74**	0.03	0.049
South Indian	**0.05**	0.005	0.005	**3.03**	0.30	0.20	**0.20**	0.02	0.05	**1.85**	0.39	0.16	**0.11**	0.001	0.001	**0.06**	0.002	0.004
Southern Ocean	**0.002**	0.0003	0.0003	**0.15**	0.01	0.01	**0.01**	0.001	0.003	**0.09**	0.02	0.01	**0.01**	0.0001	0.0001	**0.00**	0.0001	0.0002
Arctic	**0.02**	0.002	0.0020	**1.34**	0.13	0.05	**0.09**	0.01	0.02	**0.83**	0.18	0.04	**0.05**	0.0005	0.0004	**0.03**	0.001	0.002
Mediterranean	**0.18**	0.02	0.02	**10.66**	1.07	0.36	**0.92**	0.09	0.22	**6.76**	1.42	0.36	**0.37**	0.004	0.004	**0.24**	0.011	0.017
Antarctic ice sheets	**0.001**	0.0001	0.0001	**0.08**	0.007	0.003	**0.00**	0.001	0.002	**0.05**	0.01	0.003	**0.00**	0.00003	0.00003	**0.00**	0.0001	0.0001
Greenland ice sheets	**0.09**	0.01	0.01	**5.39**	0.49	0.21	**0.44**	0.04	0.10	**3.30**	0.71	0.19	**0.17**	0.002	0.002	**0.11**	0.005	0.007
Total	**2.83**	0.30	0.28	**185.32**	16.89	7.52	**12.11**	1.32	3.35	**109.89**	22.84	6.95	**6.10**	0.068	0.06	**3.69**	0.153	0.25

884 *Here the soluble element deposition using Sol-1 has been tuned by timing tuned ratios (Table 3); Sol-1 refer to mineral method after tuning, Sol-2 refer to Sillanpaa method
885 described in the methods section (2).

Main Figures 1- 15

Fig.1. Observational sites (S1-Hetian, China; S2-Tazhong, China; S3-Yu Lin, China; S4-Duolun, China; S5-Shengsi, China; S6-Hanoi, Vietnam; S7-Marnila, Philippines; S8- Balad, Iraq; S9-Balad, Iraq; S10-Taji, Iraq; S11-Eilat; S12-Cape Verde Atmospheric Observatory (CVAO); S13-Muswellbrook, Australia; S14-Richmond, Australia; S15-Tamanrasset, Algeria; S16-Banizoumbou, Niger; S17-Douz, Tunisia) **and dust-producing regions** (WAsia: West Asia; NC-As: North Central Asia; CAsia: Central Asia; SC-As: South Central Asia; EAsia:East Asia; WN-Af:North West Africa; EN-Af: North East Africa; S-NAf: Southern North Africa; SAf: Southern Africa; MWNAm: Middle North West America; SWNAm: Southern North West America; SAm1: Northern South America; SAm2: Southern South America; WAus: West Australia; EAus: East Australia)

Fig.2 Global elemental distributions (in mass percentage) in a1: Clay Mg, a2: Clay P, a3: Clay Ca, a4: Clay Mn, a5: Clay Fe, a6: Clay K, a7:, Clay Al, a8: Clay Si; b1: Silt Mg, b2: Silt P, b3: Silt Ca, b4: Silt Mn, b5: Silt Fe, b6: Silt K, b7: Silt Al, b8: Silt Si.

Fig.3 Global mean elemental percentages in (a) four-bin dust emission and (b) clay and silt fractions of soils (Bin1-4 refer to particle range listed in Table S2, clay refer to < 2um, silt refer to > 2um)

Fig.4 Percentages of elements in dust concentration （mass %）: a. Mg, b. P, c. Ca, d. Mn, e. Fe, f. K, g. Al, h. Si. Elemental % shown here are calculated using the annual mean element concentration divided by the annual mean dust concentration.

Fig.5 Ratio of mass fractions of elements in dust deposition to that in atmospheric dust : a. Mg, b. P, c. Ca, d. Mn, e. Fe, f. K, g. Al, h. Si. Elemental ratios shown here are calculated using the annual mean element deposition divided by the annual mean dust deposition.

Fig.6 Ten-year monthly variability in mean of elemental percentages in atmospheric dust (mass %) : a. Mg, b. P, c. Ca, d. Mn, e. Fe, f. K, g. Al, h. Si. Elemental monthly mean % are calculated using the monthly mean emission of each element divided by the monthly mean emission of dust.

Fig.7 Ten-year monthly variability in mean of elemental percentages in dust deposition (mass %):a. Mg, b. P, c. Ca, d. Mn, e. Fe, f. K, g. Al, h. Si. Elemental monthly mean % are calculated using the monthly mean emission of each element divided by the monthly mean emission of dust.

Fig.8 Ca/Al in Soil and ten year averaged Ca/Al ratio in dust emission, concentration and deposition. Top two (a,b) refer to ratio in clay and silt desert soil, middle one (c) refer to ratio in dust emission, and bottom two (d,e) refer to

ratio in dust concentration and deposition. Elemental annual mean % are calculated using the annual mean emission of each element divided by the annual mean emission of dust.

Fig.9 Ten year averaged Ca/Al ratio in (a) dust emission of source regions and (b) dust deposition into various ocean basins and glaciers. Elemental ratios are calculated using the annual mean emission of Ca divided by the annual mean emission of Al.

Fig.10 Comparison of observed and modeled mean fractions of elements at each site for (a) total suspended particulates (TSP) and (b) $PM_{2.5}$. (1-Hetian, China; 2-Tazhong, China; 3-Yu Lin, China; 4-Duolun, China; 5-Shengsi, China; 6-Hanoi, Vietnam; 7-Marnila, Philippines; 8-Balad, Iraq; 9-Baghdad, Iraq; 10-Taji,Iraq; 11-Eilat; 12-Cape Verde Island; 13-Muswellbrook, Australia; 14-Richmond, Australia, 15-Tamanrasset, Algeria; 16-Banizoumbou, Niger; 17-Douz, Tunisia). Here we calculate the elemental fractions and average the fractions temporally for each site and compare to observations.

Fig.11 Mean and quartile modeled and observational fractions of elements in (a) TSP (b) $PM_{2.5}$ for all sites together, the box line presents 25%, 50% and 75%, individually. Here we calculate the elemental fractions and average the fractions temporally for each site and compare to observations.

Fig.12 (a) Observational and (b) modeled dust deposition (g/m^3/year). The scale is the same for both panels. (c) A scatterplot shows the comparison between the model and observations. The correlation coefficient between observations and model results reach 0.86.

Fig.13 Percentages of elements in dust deposition（%) after tuning. It is tuned based on original percentages of elements in dust deposition in Fig. S1 by timing Obs./Mod. ratios listed in Table 3. Si did not change because there are not enough observational data available

Fig. 14 Fractional solubility of elements (soluble element / total element) in dust deposition (%):a. Mg, b. P, c. Ca, d. Mn, e. Fe, f. K, g. Al, h. Si

Fig. 15 Percentages of soluble elements in total dust deposition using(a) Sol-1 & (b) Sol-2 (‰), Sol-1 refer to mineral method after tuning, Sol-2 refer to Sillanpaa method described in the methods section (2).

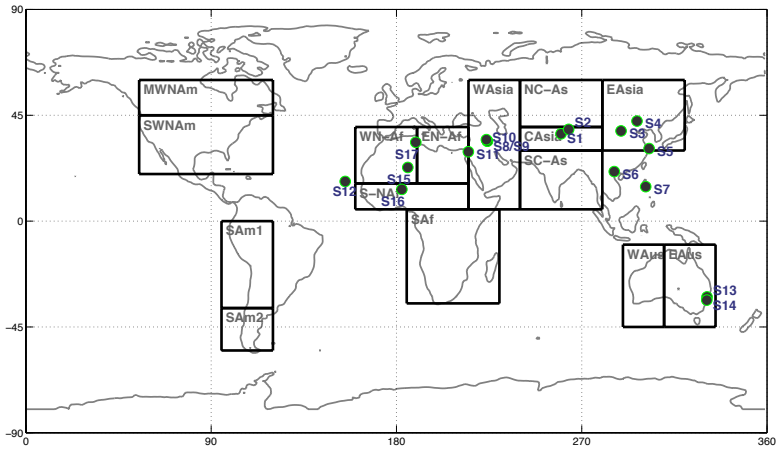

Fig.1. Observational sites (S1-Hetian, China; S2-Tazhong, China; S3-Yu Lin, China; S4-Duolun, China; S5-Shengsi, China; S6-Hanoi, Vietnam; S7-Marnila, Philippines; S8- Balad, Iraq; S9-Balad, Iraq; S10-Taji, Iraq; S11-Eilat; S12-Cape Verde Atmospheric Observatory (CVAO); S13-Muswellbrook, Australia; S14-Richmond, Australia; S15-Tamanrasset, Algeria; S16-Banizoumbou, Niger; S17-Douz, Tunisia) **and dust-producing regions** (WAsia: West Asia; NC-As: North Central Asia; CAsia: Central Asia; SC-As: South Central Asia; EAsia:East Asia; WN-Af:North West Africa; EN-Af: North East Africa; S-NAf: Southern North Africa; SAf: Southern Africa; MWNAm: Middle North West America; SWNAm: Southern North West America; SAm1: Northern South America; SAm2: Southern South America; WAus: West Australia; EAus: East Australia)

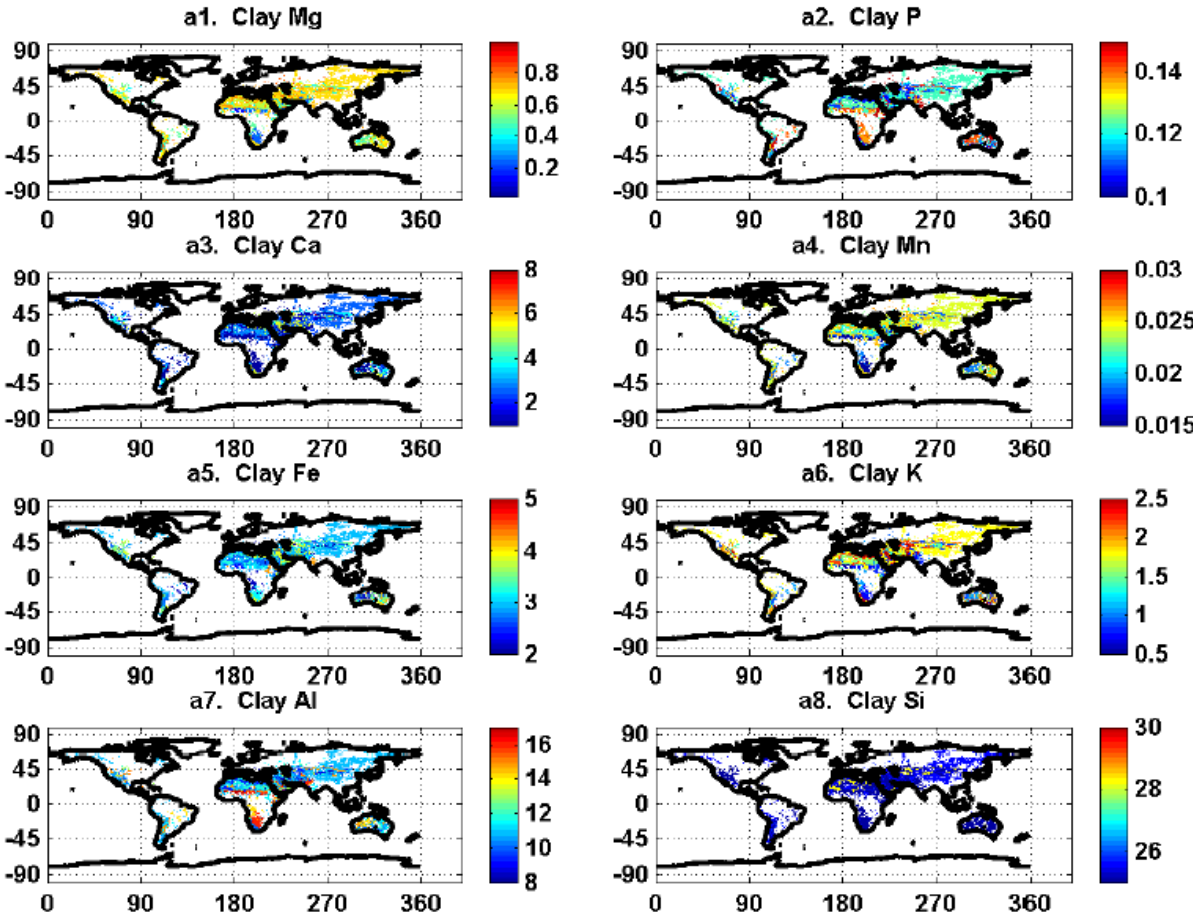

954

955 (a) in soil clay

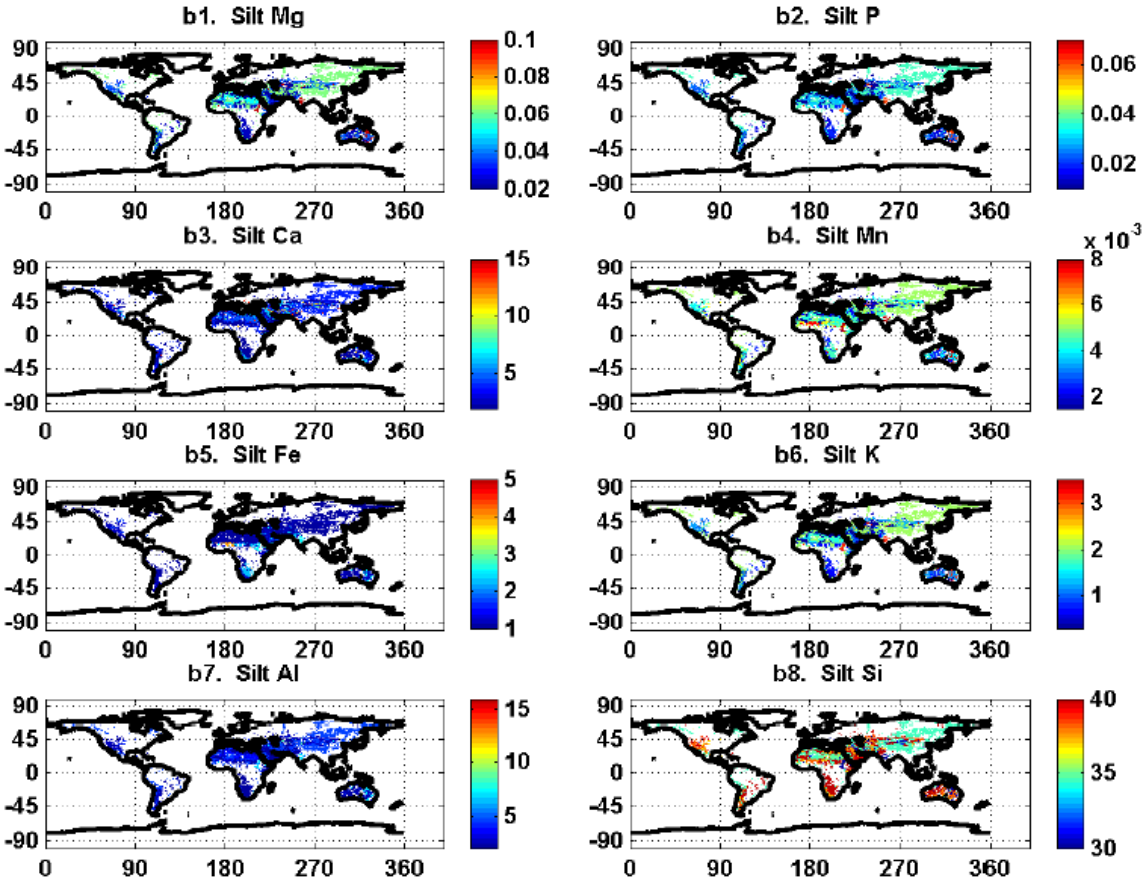

(b) in soil silt

Fig.2 Global elemental distributions (in mass percentage) in (a) soil clay, a1: Clay Mg, a2: Clay P, a3: Clay Ca, a4: Clay Mn, a5: Clay Fe, a6: Clay K, a7:, Clay Al, a8: Clay Si; (b) soil silt, b1: Silt Mg, b2: Silt P, b3: Silt Ca, b4: Silt Mn, b5: Silt Fe, b6: Silt K, b7: Silt Al, b8: Silt Si.

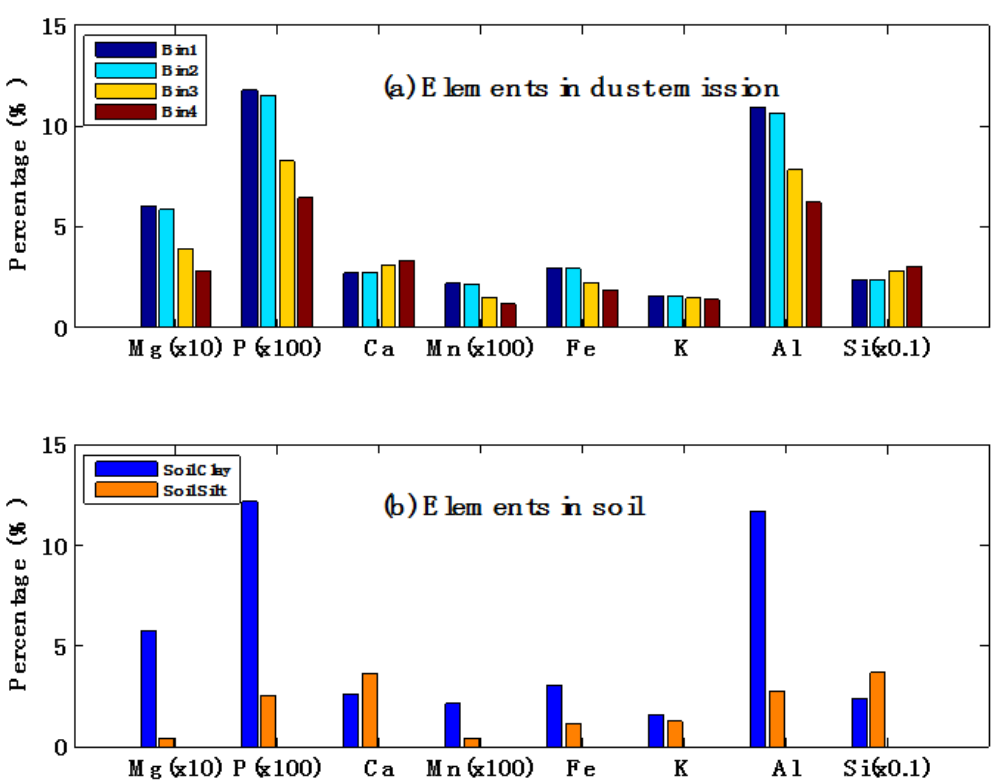

961

962 Fig.3 Global mean elemental percentages in (a) four-bin dust emission and (b) clay and silt fractions of soils (Bin1-4

963 refer to particle range listed in Table S2, clay refer to < 2um, silt refer to > 2um)

964

965

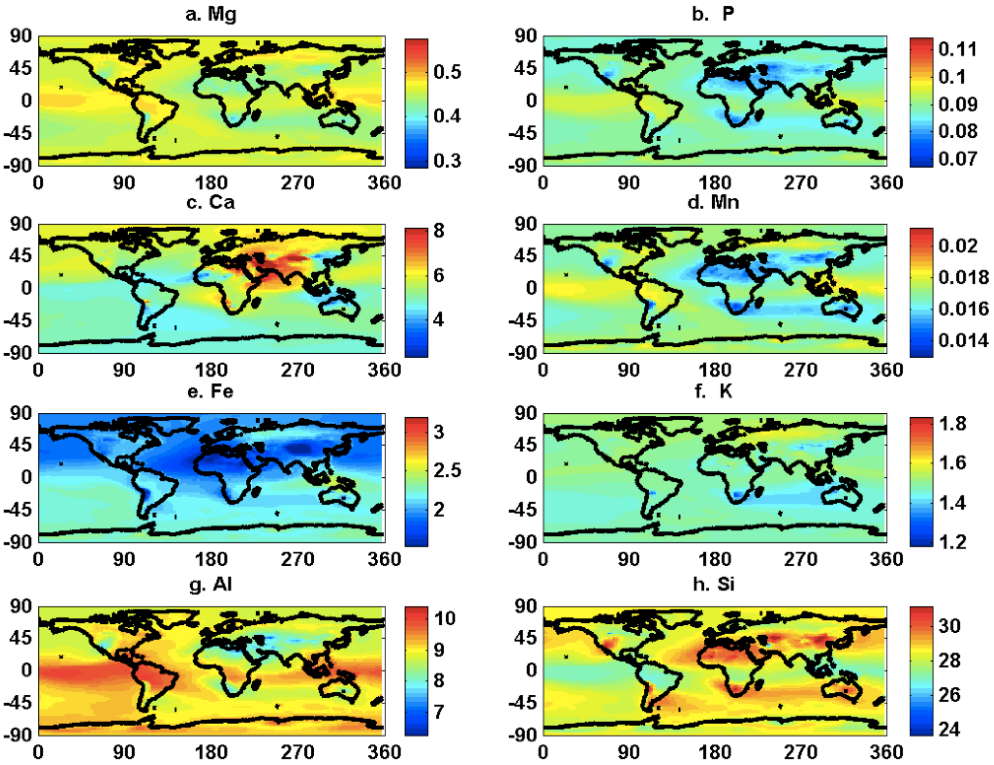

966

967 Fig.4 Percentages of elements in dust concentration （mass %）: a. Mg, b. P, c. Ca, d. Mn, e. Fe, f. K, g. Al, h. Si.
968 Elemental % shown here are calculated using the annual mean element concentration divided by the annual mean
969 dust concentration.

970

971

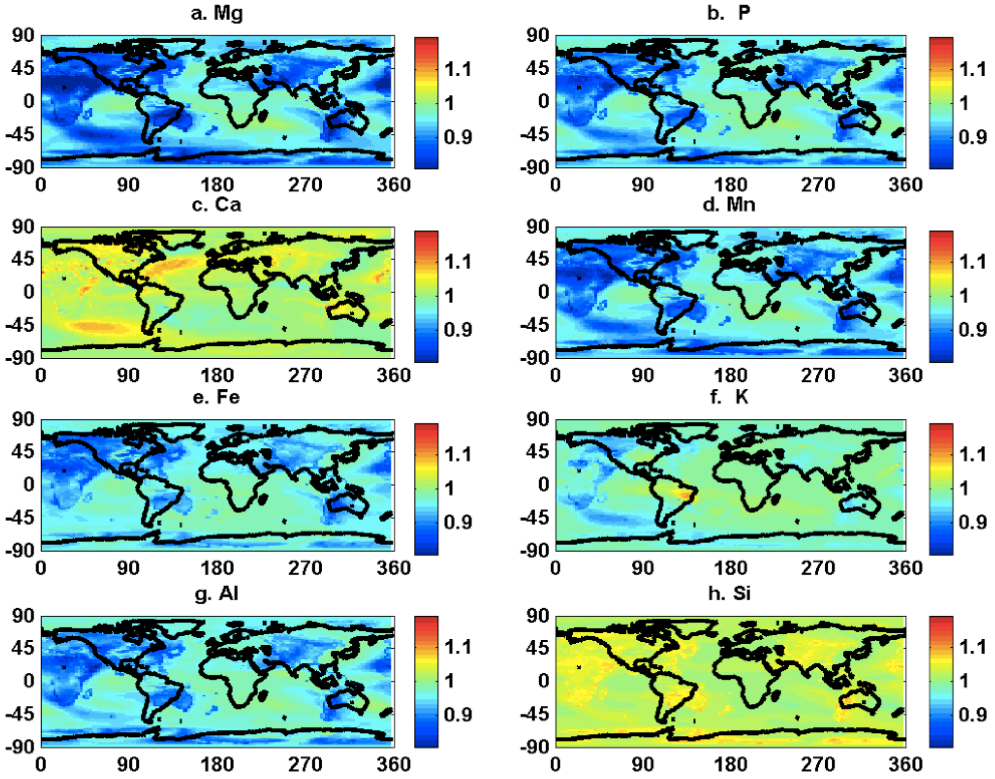

972

973 Fig.5 Ratio of mass fractions of elements in dust deposition to that in atmospheric dust : a. Mg, b. P, c. Ca, d. Mn, e.
974 Fe, f. K, g. Al, h. Si. Elemental ratios shown here are calculated using the annual mean element deposition divided
975 by the annual mean dust deposition.

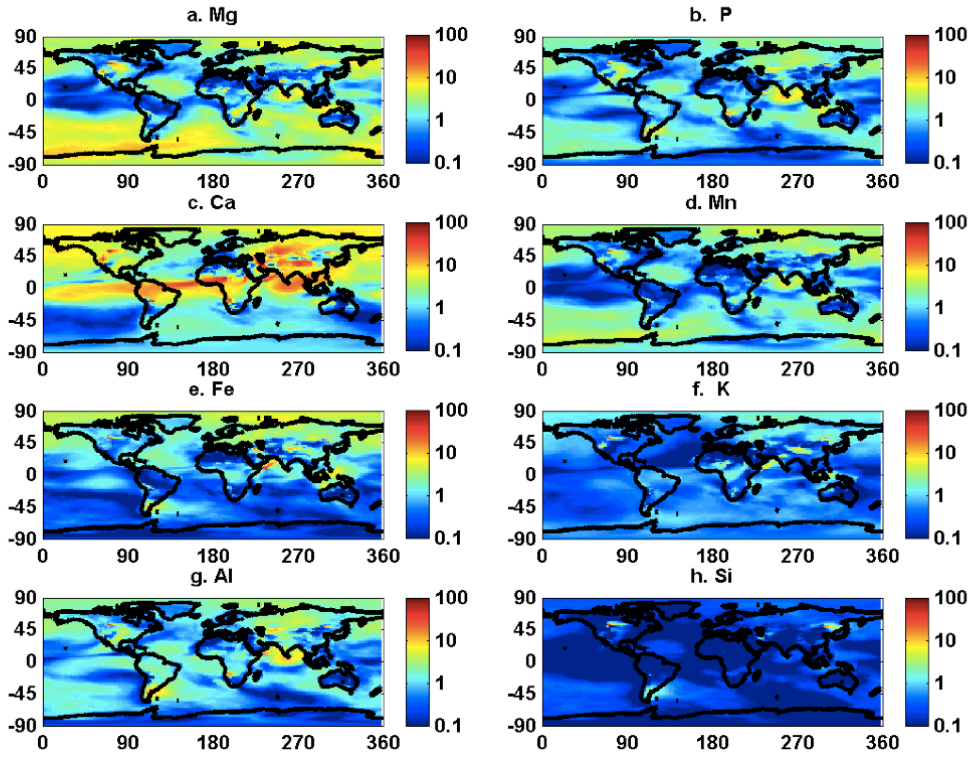

976

977 Fig.6 Ten-year monthly variability in mean of elemental percentages in atmospheric dust (mass %) : a. Mg, b. P, c.
978 Ca, d. Mn, e. Fe, f. K, g. Al, h. Si. Elemental monthly mean % are calculated using the monthly mean emission of
979 each element divided by the monthly mean emission of dust.

980

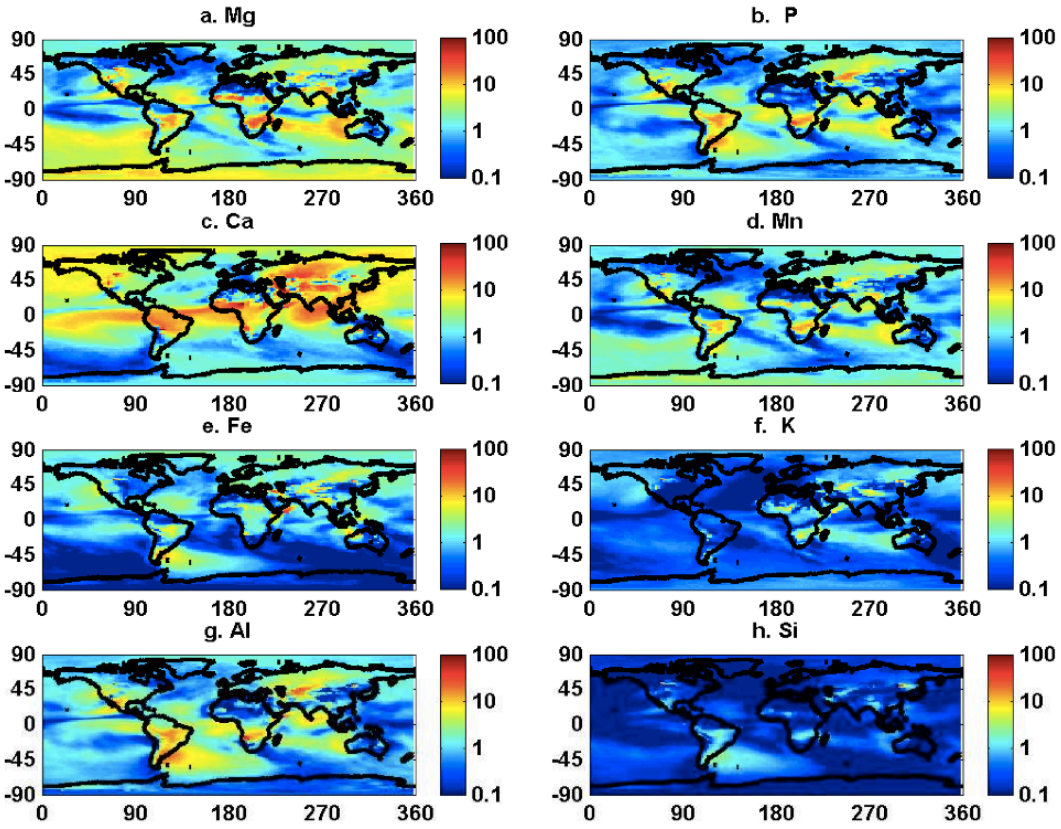

981

982 Fig.7 Ten-year monthly variability in mean of elemental percentages in dust deposition (mass %):a. Mg, b. P, c. Ca,
983 d. Mn, e. Fe, f. K, g. Al, h. Si. Elemental monthly mean % are calculated using the monthly mean emission of each
984 element divided by the monthly mean emission of dust.

985

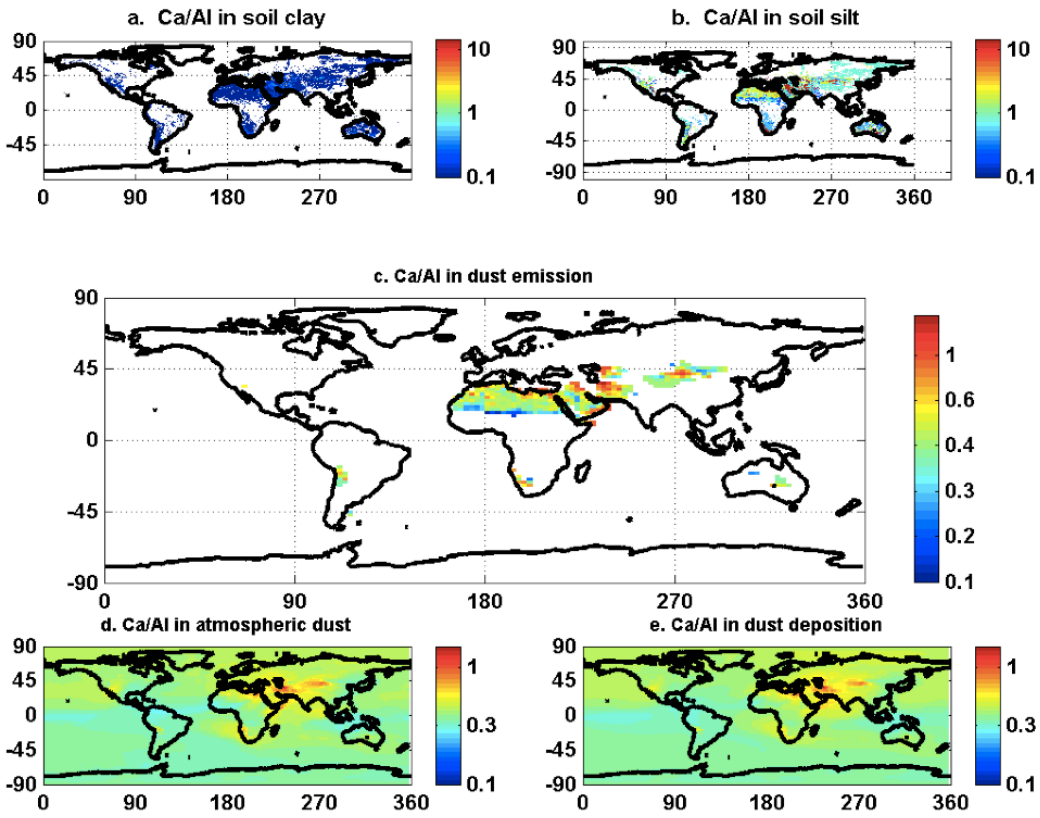

986

987

988 Fig.8 Ca/Al in Soil and ten year averaged Ca/Al ratio in dust emission, concentration and deposition. Top two (a,b)
989 refer to ratio in clay and silt desert soil, middle one (c) refer to ratio in dust emission, and bottom two (d,e) refer to
990 ratio in dust concentration and deposition. Elemental annual mean % are calculated using the annual mean
991 emission of each element divided by the annual mean emission of dust.

992

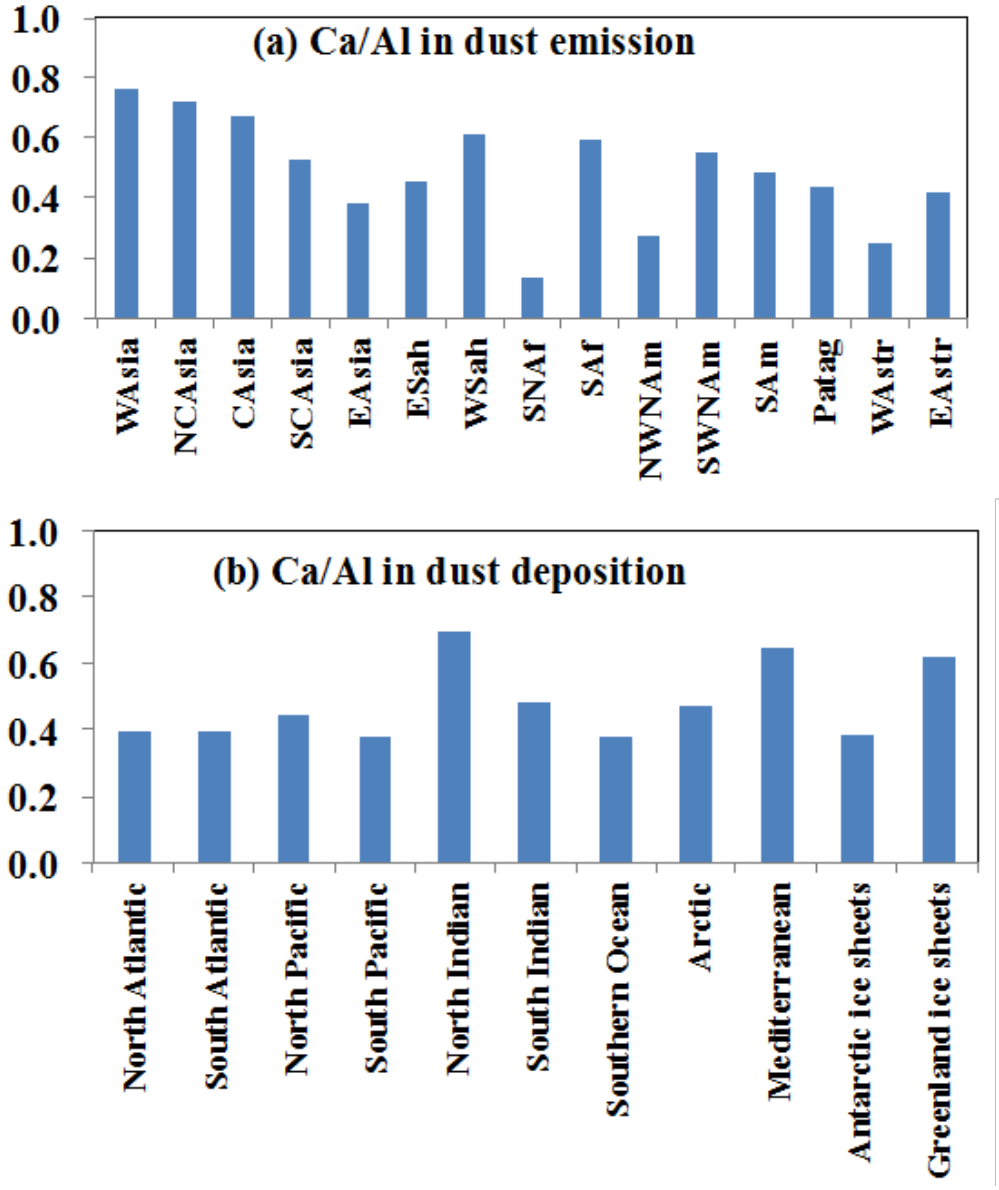

993

994 Fig.9 Ten year averaged Ca/Al ratio in (a) dust emission of source regions and (b) dust deposition into various ocean
995 basins and glaciers. Elemental ratios are calculated using the annual mean emission of Ca divided by the annual
996 ean emission of Al.

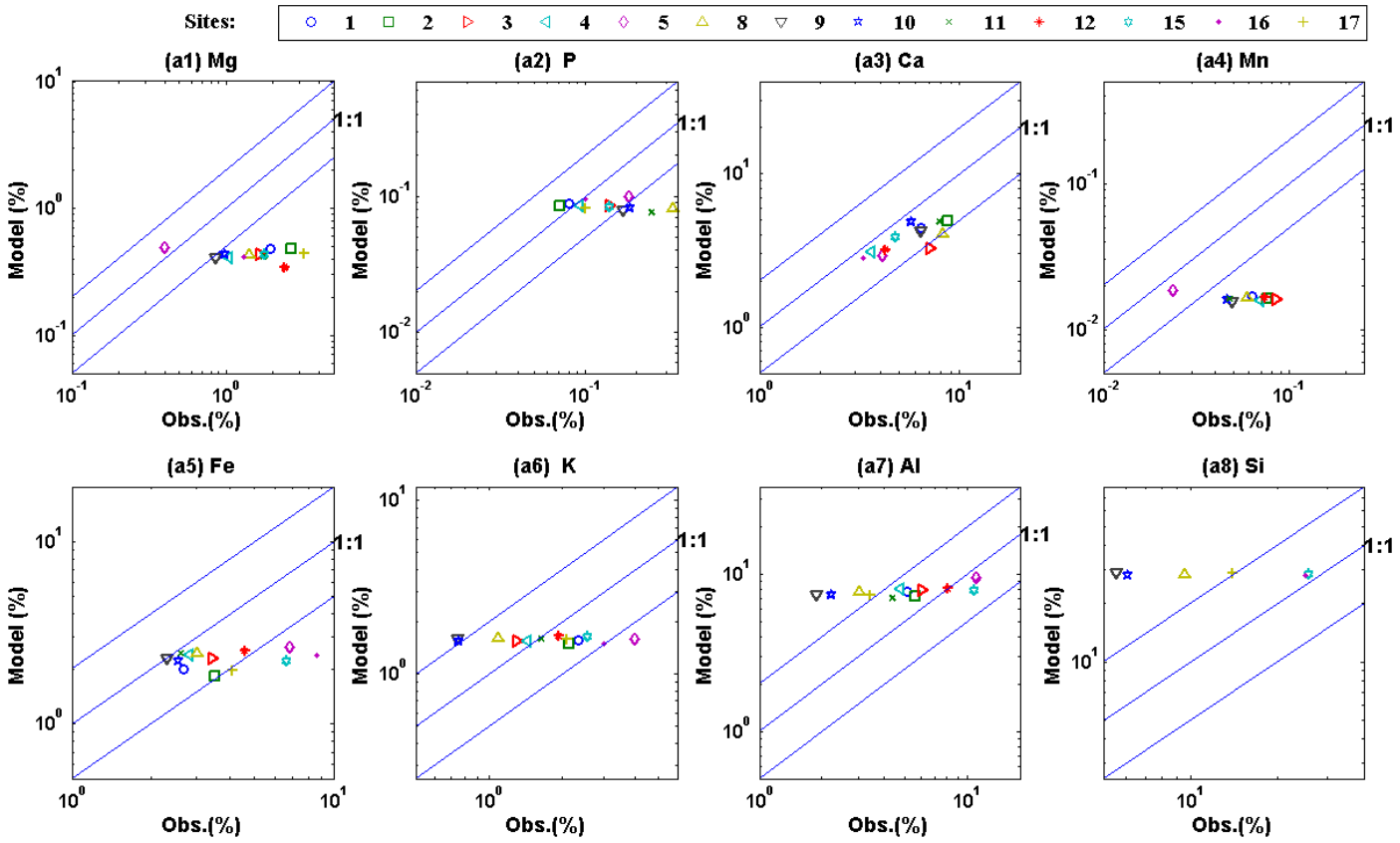
Sites: 1 2 3 4 5 8 9 10 11 12 15 16 17
(a1) Mg
(a2) P
(a3) Ca
(a4) Mn
(a5) Fe
(a6) K
(a7) Al
(a8) Si
Model (%)
Obs.(%)
1:1

997

998

(a) TSP

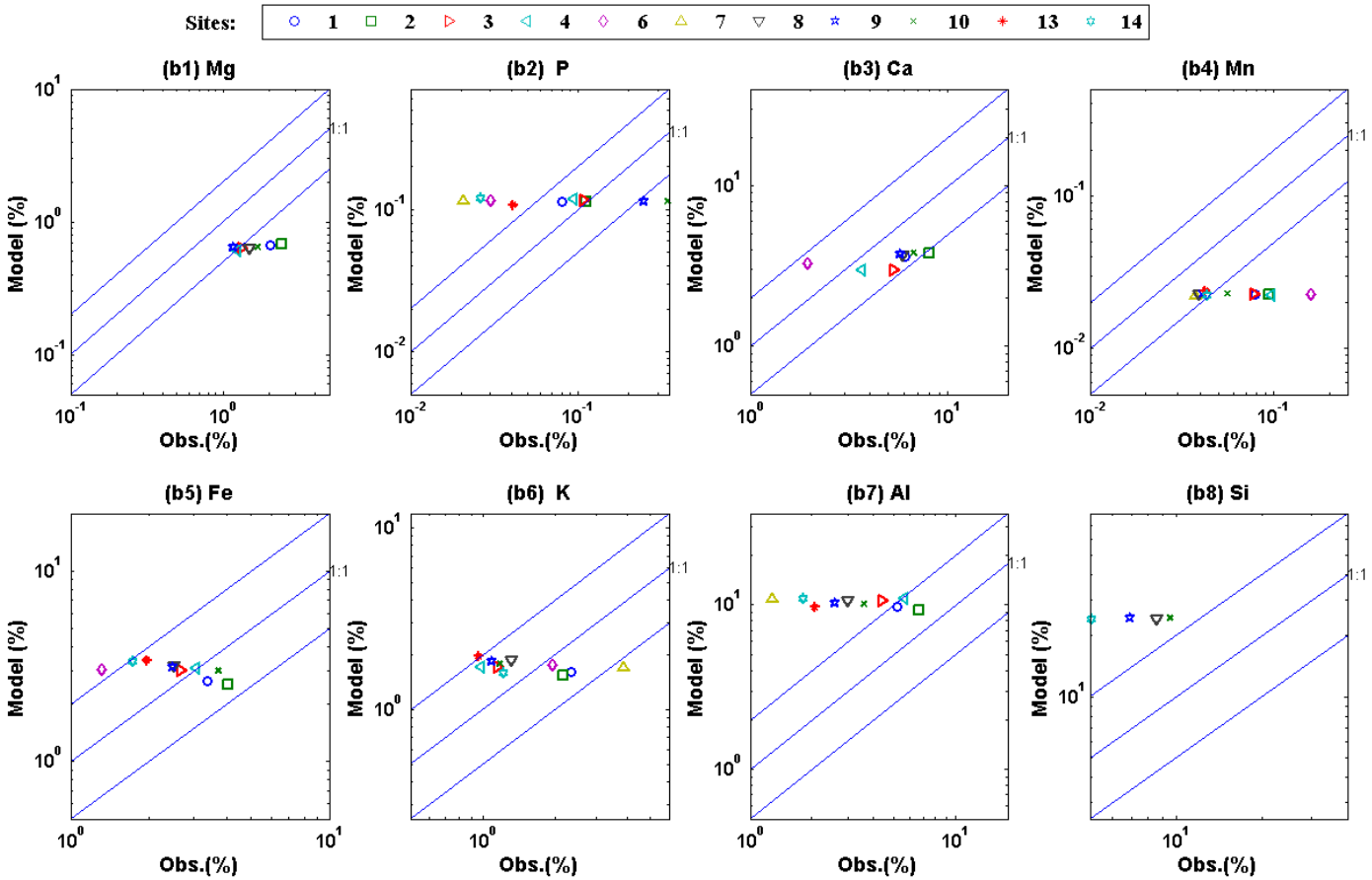

(b) $PM_{2.5}$

Fig.10 Comparison of observed and modeled mean fractions of elements at each site for (a) total suspended particulates (TSP) and (b) $PM_{2.5}$. (1-Hetian, China; 2-Tazhong, China; 3-Yu Lin, China; 4-Duolun, China; 5-Shengsi, China; 6-Hanoi, Vietnam; 7-Marnila, Philippines; 8-Balad, Iraq; 9-Baghdad, Iraq; 10-Taji,Iraq; 11-Eilat; 12-Cape Verde Island; 13-Muswellbrook, Australia; 14-Richmond, Australia, 15-Tamanrasset, Algeria; 16-Banizoumbou, Niger; 17-Douz, Tunisia). Here we calculate the elemental fractions and average the fractions temporally for each site and compare to observations.

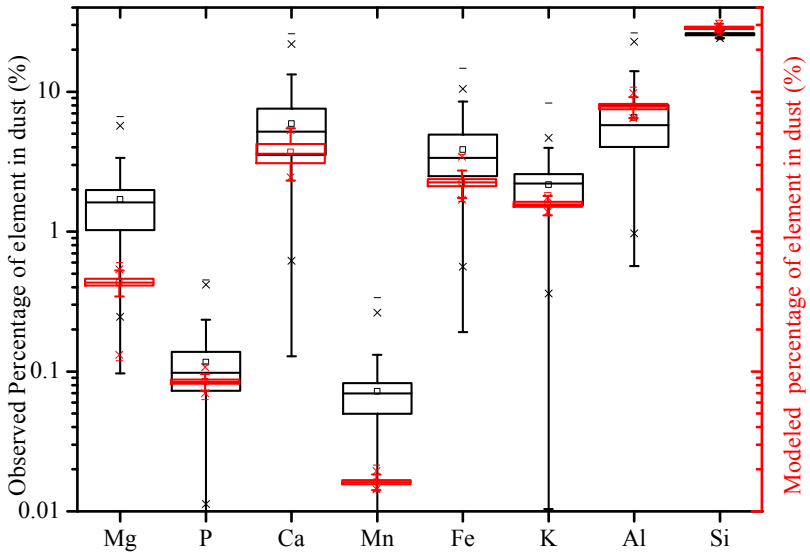

(a) TSP

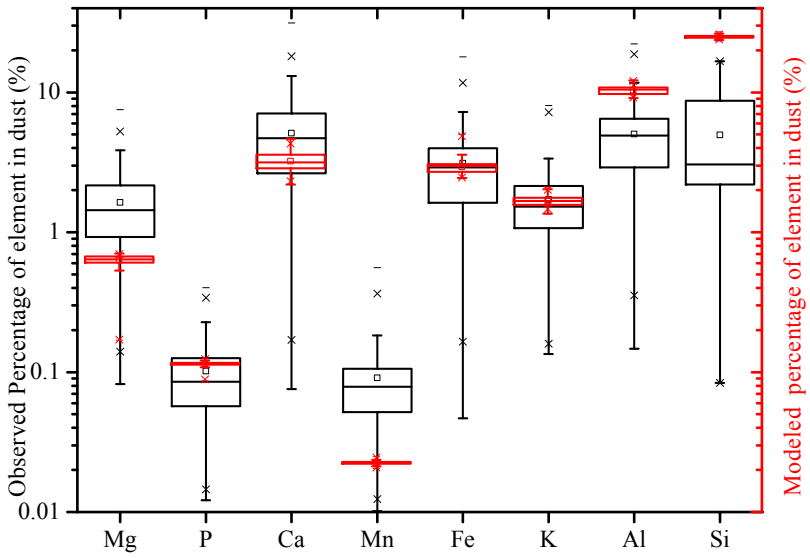

(b) $PM_{2.5}$

Fig.11 Mean and quartile modeled and observational fractions of elements in (a) TSP (b) $PM_{2.5}$ for all sites together, the box line presents 25%, 50% and 75%, individually. Here we calculate the elemental fractions and average the fractions temporally for each site and compare to observations.

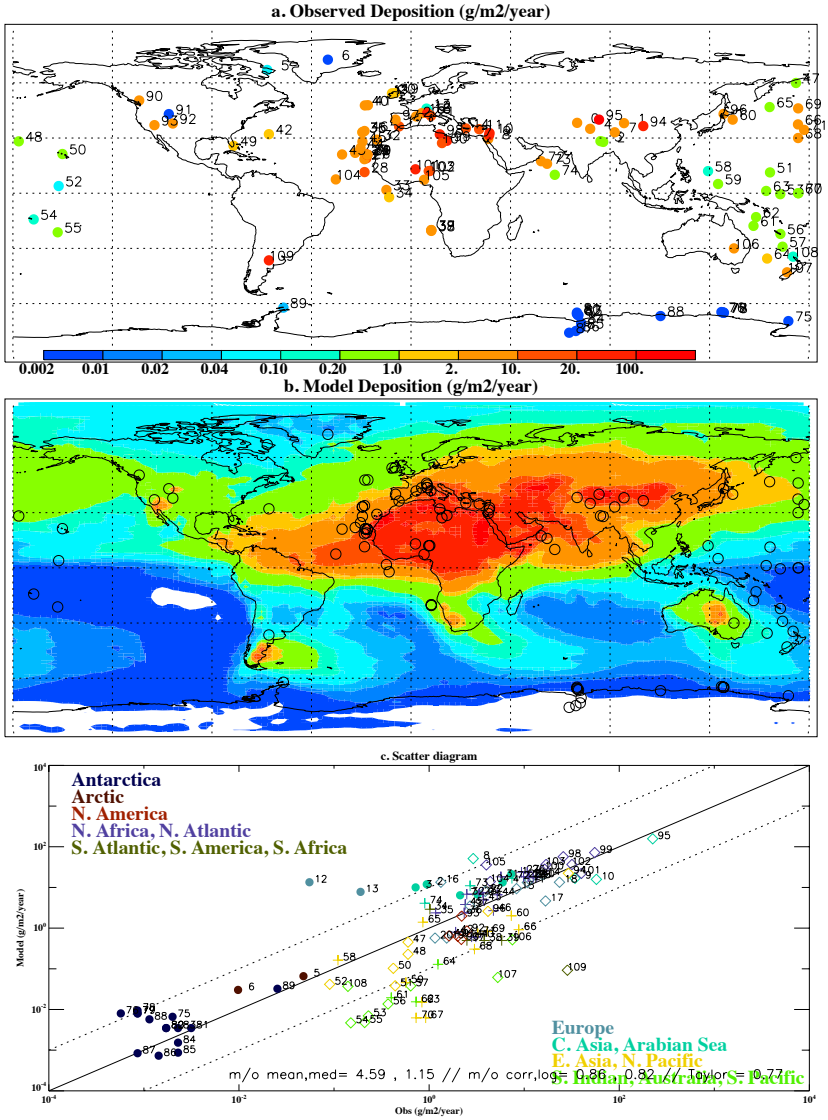

1013

1014 Fig.12 (a) Observational and (b) modeled dust deposition (g/m^3/year). The scale is the same for both
1015 panels. (c) A scatterplot shows the comparison between the model and observations. The correlation
1016 coefficient between observations and model results reach 0.86.

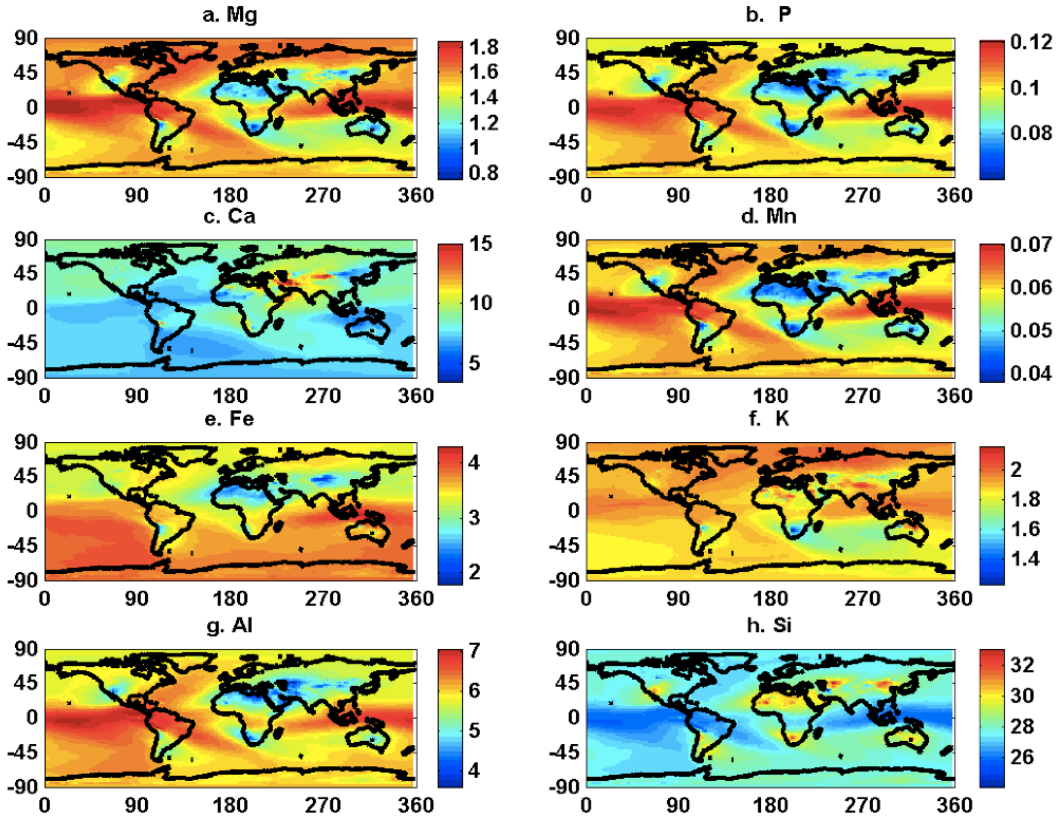

1017

1018 Fig.13 Percentages of elements in dust deposition（%) after tuning. It is tuned based on original
1019 percentages of elements in dust deposition in Fig. S1 by timing Obs./Mod. ratios listed in Table 3. Si
1020 did not change because there are not enough observational data available

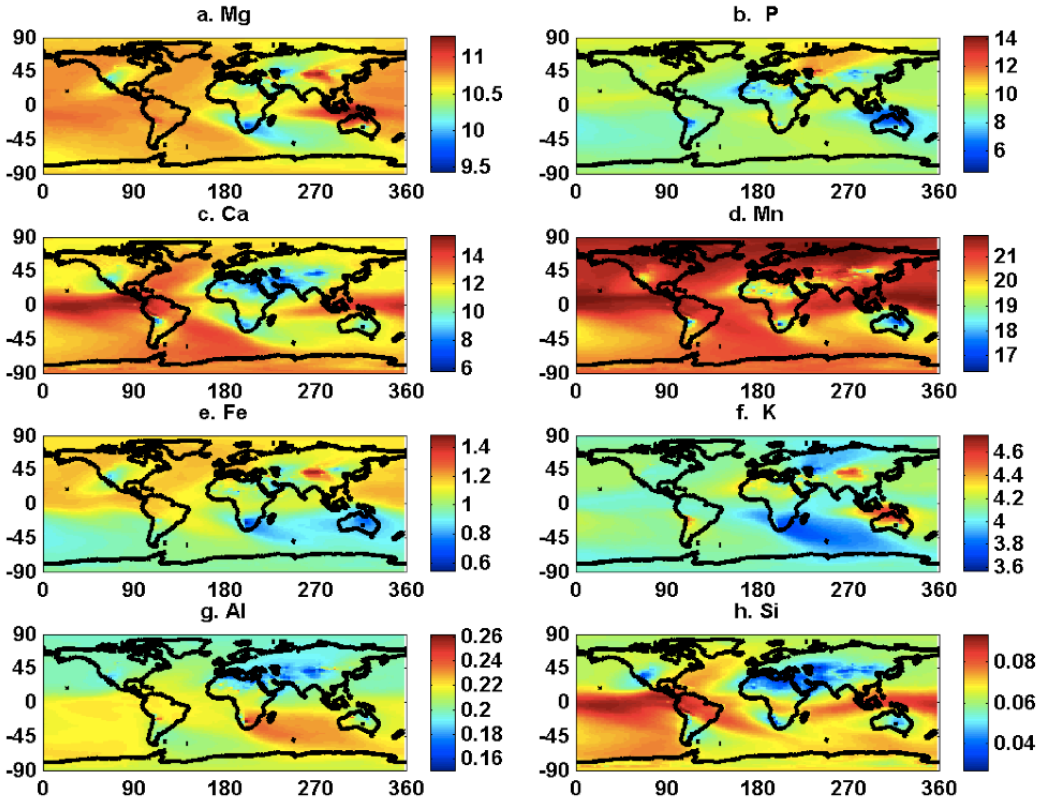

1021

1022 Fig. 14 Fractional solubility of elements (soluble element / total element) in dust deposition (%):a. Mg, b.
1023 P, c. Ca, d. Mn, e. Fe, f. K, g. Al, h. Si

1024

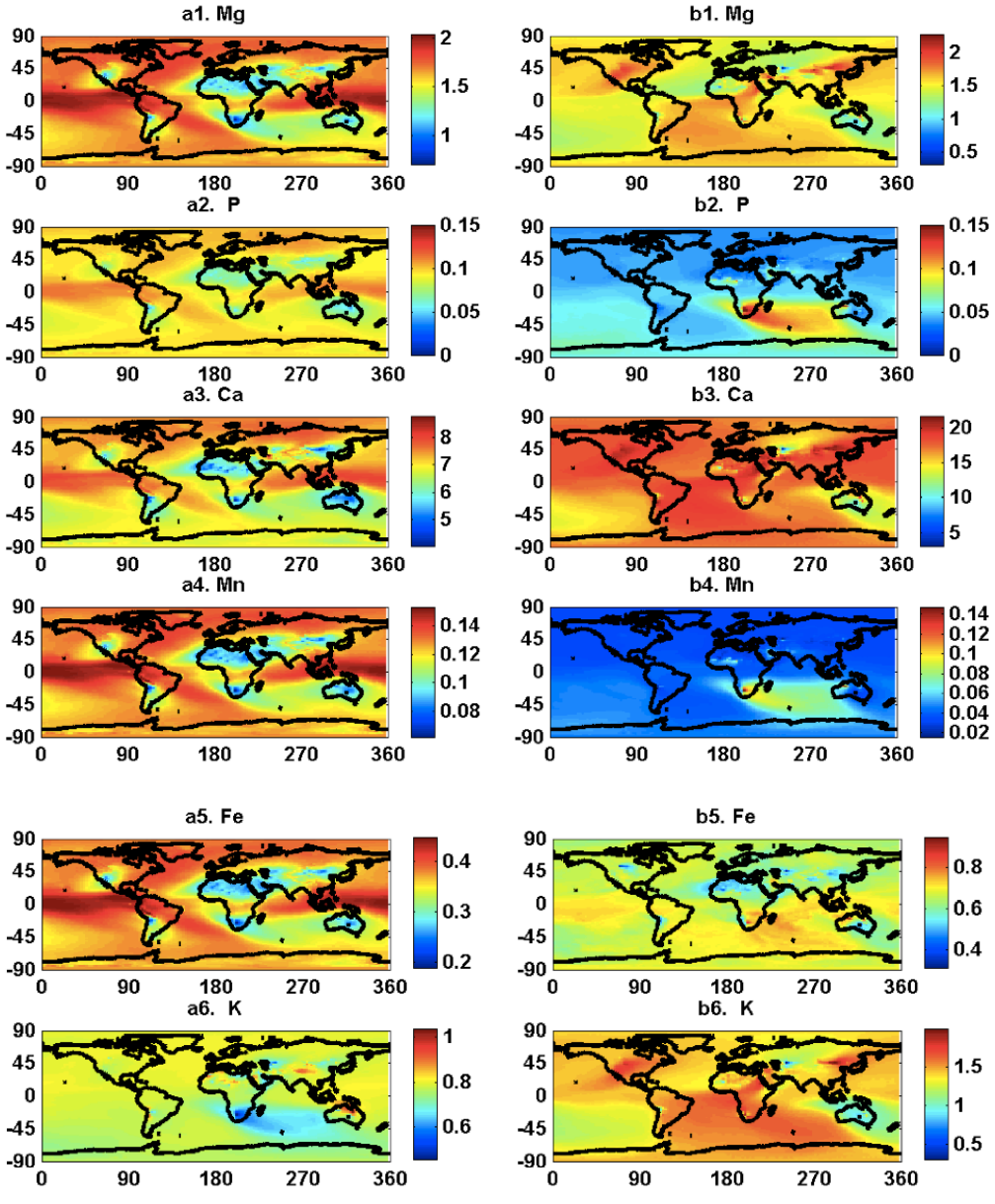

Fig. 15 Percentages of soluble elements in total dust deposition using(a) Sol-1 & (b) Sol-2 (‰), Sol-1 refer to mineral method after tuning, Sol-2 refer to Sillanpaa method described in the methods section (2).